

# Bulletin of Volcanology

## Historical explosive activity of Mount Melbourne Volcanic Field (Antarctica) revealed by englacial tephra deposits --Manuscript Draft--

<b>Manuscript Number:</b>	BUVO-D-23-00013R1	
<b>Full Title:</b>	Historical explosive activity of Mount Melbourne Volcanic Field (Antarctica) revealed by englacial tephra deposits	
<b>Article Type:</b>	Research Article	
<b>Corresponding Author:</b>	Alessio Di Roberto, Ph.D Istituto Nazionale di Geofisica e Vulcanologia Sezione di Pisa Pisa, Italy ITALY	
<b>Corresponding Author Secondary Information:</b>		
<b>Order of Authors:</b>	Paola Del Carlo Alessio Di Roberto, Ph.D Giuseppe Re, PhD Paul G. Albert Victoria C. Smith, PhD Gaetano Giudice Graziano Larocca Bianca Scateni Andrea Cannata, PhD	
<b>Funding Information:</b>	Ministero dell'Istruzione, dell'Università e della Ricerca (PNRA16_00055 - A3)	Dr. Alessio Di Roberto
	Ministero dell'Istruzione, dell'Università e della Ricerca (PNRA 14_00011)	Not applicable
<b>Abstract:</b>	<p>Five tephra layers named BRH1 to 5 have been sampled in an ice cliff located on the north-eastern flank of Mount Melbourne (northern Victoria Land, Antarctica). The texture, componentry, mineralogy and major- and trace-elements compositions of glass shards have been used to characterise these layers. These properties suggest that they are primary fall deposits produced from discrete eruptions that experienced varying degrees of magma/water interaction. The major- and trace-element glass shard compositions analyses on single glass shards indicate that Mount Melbourne Volcanic Field is the source of these tephra layers and the geochemical diversity highlights that the eruptions were fed by compositionally diverse melts that are interpreted to be from a complex magma system with a mafic melt remobilizing more evolved trachy-andesitic to trachytic magma pockets. Geochemical compositions, along with textural and mineralogical data, have allowed correlations between two of the englacial tephra and distal cryptotephra from Mount Melbourne, recovered within a marine sediment core in the Edisto Inlet (~280 km northeast of Mount Melbourne), and provide constrain these englacial tephra layers to between the 3rd and the 4th centuries CE.</p> <p>This work provides new evidence of the intense historical explosive activity of the Mount Melbourne Volcanic Field and better constrains the rates of volcanism in northern Victoria Land. These data grant new clues on the eruptive dynamics and tephra dispersal, and considerably expand the geochemical (major and trace elements) dataset available for the Mount Melbourne Volcanic Field. In the future, this will facilitate the precise identification of tephra layers from this volcanic source and will help define the temporal and spatial correlation between Antarctic records using tephra layers. Finally, this work also yields new valuable time-stratigraphic marker horizons for future dating, synchronisation and correlations of different paleoenvironmental and</p>	

	paleoclimatic records and across large regions of Antarctica.
<b>Response to Reviewers:</b>	<p>BUVO-D-23-00013 Title: Historical explosive activity of Mount Melbourne volcano (Antarctica) revealed by englacial tephra.</p> <p>Editor: Of particular importance, you need to strengthen the arguments for the layers being primary tephra. This is fundamental. At present, you discuss this issue late on the paper (section 4.2). It needs to be moved to an earlier position and strengthened. The layers are highly unusual, being formed individually of several compositionally different sideromelane clasts. That might be explained by evacuation of a stratified chamber (you need to discuss this) but, as the reviewer suggests, it may also be due to surface reworking of several compositionally disparate sources. I have a field photo that shows the ice outcrop with your tephra layers and they seem to dip away from Baker Rocks as if they are successive ice bedload layers. Can you describe whether there is any abrasion of the clasts or are they so fragile &amp; spinose that they cannot possibly be reworked (and are therefore primary)? You describe them as fall layers yet they sound like poorly sorted mixtures of ash &amp; lapilli, which is not like fall (too much fine matrix). Can you clarify better why you think they are fall layers?</p> <p>Reply:</p> <p>We agree. The “primary nature” of the layers only after the Results chapter since we would define (or confirm) their characteristics only after the textural and geochemical analysis. We have moved this section earlier to “3.1 Texture and components of tephra layers” just before the “Results” section, and refer back to it later in the paper.</p> <p>In addition, in the Materials and methods chapter, we added a paragraph explaining that each sample is a “bulk” of the tephra layer thickness. In fact, due to the extreme sampling conditions, it was not possible to sub-sample each tephra layer at different stratigraphic heights and consequently study possible stratification with relative variation in grain size, composition, etc. relative to changes in the eruptive style, dynamics or in the composition of the magma feeding the eruptions. The samples were collected still embedded in the ice, which was then melted to recover the clastic fraction.</p> <p>Again, as for the “primary nature” of the studied tephra, from the point of view of texture, we better highlight that glass fibres or Pele’s hairs were preserved in the deposits which is impossible in the case of re-sedimentation. The same for other fragile structures such as glass tips or glass coatings around crystals. In addition, particles show no rounding, abrasions, or surficial weathering, which is all indicative of re-sedimentation.</p> <p>From the geochemical side, besides the glass composition of studied samples being bimodal or spread on a compositional field, these (especially on the trace elements variation diagrams) clearly plot on the same geochemical lineage indicating they are geochemically linked and derive all from the same volcanic system. We explained this in the Discussion chapter: “The overall chemical variability (ranging from basalts through to trachytes) and in particular the observed clustering of the erupted volcanic glass compositions along the overall evolutionary trend might indicate that the successive eruptions were fed by a complex and vertically extensive magma storage region beneath the source volcano. Interestingly, apart from BRH4, all the remaining BRH tephra deposits comprise a basaltic glass component, and the interaction of the mafic melt with more evolved trachy-andesitic to trachytic magma pockets, or mush, is the likely trigger of these eruptions”. This behaviour is quite frequent in many volcanic systems where explosive eruptions are fed by bimodal magmas (e.g. basalts and trachytes), or by chemically zoned magma batch (covering a wide and continuous compositional spectrum). Just to mention some examples: Upper and Lower Pollara eruption, on Salina island, Aeolian Islands; several historical eruptions of La Palma, Canary Islands; most of the eruptions from Iceland volcanoes; Izu-Bonin Arc and many others.</p> <p>Also, you use descriptors like 'Mt Melbourne volcanic complex' and 'Mt Melbourne volcanic province'. That is liable to cause confusion since the region has already been divided stratigraphically into the Melbourne Volcanic Province and the Mt Melbourne Volcanic Field (both part of the McMurdo Volcanic Group; see Sm &amp; Rocchi, 2021 (GSL Mem)). If you disagree with that terminology, please discuss why, and how you</p>

are using your preferred terms.

Reply: We agree and have changed throughout.

I also recommend that you incorporate the results of the study by Smellie et al (2023; Frontiers - see annotated m/s). I know it wasn't published when you submitted your paper but that paper is relevant to your study and is now available.

Reply: Done.

Like the reviewer, I was also confused by the layout of the data in the supplementary table, so it needs better page/table descriptors (e.g. what are pages labelled 1, 2, 3, 4, 5?; what is 'MPI-DING?').

Reply: Done. Supplementary material has been reorganised, we added some references in it and explained the content. For instance, MPI-DING indicates the composition of standard glasses provided by Max-Planck-Institut für Chemie that are widely used as reference glasses in EPMA analyses.

Reviewer #2: The authors have a complicated and potentially interesting story here but much needs to be addressed and clarified for this paper to be ready to publish. In the attached manuscript are a number of specific comments but I will summarize the main problems here.

More information is required for me to believe that each of these 5 layers are in fact tephra layers. These layers are undoubtedly made up of volcanic particles but more characterization is needed for them to become discrete and correlated tephra layers. Tephra is a general term for airborne pyroclastic material ejected during the course of a volcanic eruption (Thorarinsson, 1981). This could be a single eruptive event or multiple eruptions over a short period of time from the same vent.

Reply: See the comment above.

I am not sure these 5 layers are fall deposits from a single source. The bimodal compositions bother me. I do not see how the basalt and trachytes are linked to each other.

The composition of the particles in the layers are strangely similar despite not showing much chemical affinity or to each other. For instance in Layer 1, Ca is higher (~11 wt.%) in the basalt and considerably lower in the trachyte (~2 wt. %). There is only a small Eu anomaly.

Reply: See the comment above. As can be clearly seen from the variation diagrams presented in the ms, the composition of each of the BRH tephra and those in the literature from Mount Melbourne define a clear and continuous evolutionary trend from the basanite to trachyte composition fields. The basanite (which has a composition quite similar in all the studied samples) is the "parent" glass of the other compositions, in the sense that it represents the primitive term from which the more evolved compositions evolved (see comment above). This does not mean that trachyte X directly evolved from the basanite X contained in the same layers (see the comment just below, and have tried to explain this better in the discussion.

I think the authors need to show that there is geochemical evolution from one tephra layer to the other to confirm that each of the 5 trachytes evolved from a basalt to a trachyte over a very short period of time (100-200 years).

Reply: We have added in the ms: "The overall chemical variability (ranging from basalts through to trachytes) and in particular the observed clustering of the erupted volcanic glass compositions along the overall evolutionary trend might indicate that the successive eruptions were fed by a COMPLEX AND VERTICALLY EXTENSIVE MAGMA STORAGE REGION BENEATH THE SOURCE VOLCANO..." and that "tephra deposits comprise a basaltic glass component, and the interaction of the mafic melt with more evolved trachy-andesitic to trachytic magma pockets, or mush, is the likely trigger of these eruptions."

Our interpretation is that a basanite magma TRIGGERED or REMOBLIZED multiple and different trachytic and trachy-andesitic magma batches that had already evolved

and resided in different portions of the volcanic system of Mount Melbourne. This behaviour is typical in volcanic systems erupting both evolved and mafic terms (see for instance La Soufriere, La Martinica, Tenerife, etc.). Therefore, we do not understand these perplexities.

Would it be more reasonable to assume that there are multiple tephra from multiple volcanoes?

Reply: Literature data clearly show that the composition of Late Pleistocene to Holocene products of the other volcanoes of northern Victoria Land, such as The Pleiades or Mount Rittmann, plot on completely different chemical trend and clearly distinguishable from Mount Melbourne products (see Di Roberto et al. 2023 and references therein). The similar composition of the tephra presented in this paper is consistent with them being from the same source - Mt. Melbourne.

2) I am not sure the correlations and subsequent ages are robust enough. Cherry picking data to make it match distal tephra and then saying the basalt is missing because of distance and changes in winds is possible but not 5 times in a row. If there was basaltic data in the marine record then it would be more plausible. It would be great to correlate grain size with composition.

Reply: There is no "Cherry-picking" in the paper. We simply report that the tephra recently found in the Ross Sea sediments at Cape Hallett (Di Roberto et al. 2023) have IDENTICAL major and trace element compositions with two of the five tephra studied here (BRH3 and BRH5), but these lack the less evolved basanite component. Unless there is a very intense basaltic explosive eruption, it is quite difficult for basaltic ash to be dispersed more than a few tens of km from the source, and up to c. 280 km (the distance between Cape Hallett and Mount Melbourne). This is inherently linked to eruption dynamics, physical properties of basaltic magmas, plume height, etc. This is now discussed in more detail in the ms.

The differential distribution of ash with different compositions during a bimodal eruption is a common feature. An example is basaltic and rhyolitic ash dispersal in bimodal Icelandic eruptions.

Are all the basaltic particles larger than the fine ash?

Reply: In our deposits, the basaltic particles are always larger than trachytic pumices. We also specified in the ms that the mafic glass component is associated with the black glassy and fluidal particles.

3) I would like to see a more complete particle analysis comparing the size, shape and color of glass shards to composition. Is it completely mixed or are certain morphologies associated with specific compositions.

Reply: See comment above. The relation between texture and composition of different components is reported in the ms.

4) The supplemental material needs a lot more information. Here is a link to the Commission on Tephrochronology Community-based Recommendations for tephra data.

[https://www.google.com/url?q=https://earthchem.org/communities/tephra/&source=gm ail-imap&ust=1682007225000000&usg=AOvVaw3OFzNt4J\\_J6qFP\\_2vpobuu](https://www.google.com/url?q=https://earthchem.org/communities/tephra/&source=gm ail-imap&ust=1682007225000000&usg=AOvVaw3OFzNt4J_J6qFP_2vpobuu)  
I would follow their templates on how to organize data and provide the necessary meta data.

I found it very difficult to connect the EPMA shard analysis to the LA-ICP-MS data and think more information is needed to connect these two data sets.

Reply: We have inserted a sentence within the LA-ICP-MS methods to clarify how the two datasets are connected. Where glass shards were individually mapped (gridded) within an epoxy mount, the analyses are labelled with a row letter (A, B, or C) and shard number. Doing so meant that we were able to ensure that EMP and LA-ICP-MS were conducted on precisely the same particle/shard. Consequently, the shard specific SiO<sub>2</sub> content (EMP analysis) was used as the internal standard for the LA-ICP-MS analysis and calculating the trace element contents.

Where individual glass shards were analysed within un-mapped (bulk) epoxy mounts, the average SiO<sub>2</sub> content of the relevant compositional components, was used as the internal standard to calculate the trace element contents. These average internal calibration values were assessed by monitoring the Si/Ca ratios from the EMP and LA-ICP-MS analyses.

In the supplementary information, we have highlighted the compositional classifications/component of the individual analyses in the EMP and LA-ICP-MS datasets, highlighting the sample averages, where used as the internal standard for the trace element analysis, making it clear how the dataset are integrated. We have also added a column in the trace element data sheet which clearly states the SiO<sub>2</sub> content converted to ppm and used as the internal standard, and again this can be traced to the major element datasheet.

5) The geochemical plots are way too busy. I would plot each layer separately and then make 1 plot with all of the data. The data presented for Mt. Melbourne is trachy-basalt and trachyte with nothing in between. The glass compositions in this paper run the whole composition range from basanite and basalt to trachyte. More data is needed to fill in the gaps. The only eruption I have seen with >20 wt% SiO<sub>2</sub> variation was Oruanui and it was only composed of ~1% basalt by volume.

Reply: We respectfully disagree. The overlapping chemical nature of the BRH deposits is an important feature well reflected in the existing plots, it demonstrates that the successive eruptions tap similar magma compositions and likely derive from the same volcanic source region. Successive plots for individual layers would require too many figures. We have inserted some zoomed-in captions to the plots to help better resolve some of the overlapping compositions, particularly in relation to data comparisons between the BRH and BIT tephra.

In terms of the chemical heterogeneity, tapping of compositionally distinct, yet co-genetic, magmas is not uncommon, please see response above to the editors comments.

Reviewer #3: Dear Authors

I have read with interest your manuscript which provides compelling and strong data about recent tephra embedded within the Mt Melbourne ice glaciers and which may represent the deposits of the youngest preserved eruptions of this volcano, long debated as to be regarded as active and about the age of the last eruption. Geochemical correlations presented suggest that the tephra may be as young as the 3rd-4th century CE, which indeed would come as a clear indication of an active volcano. I have no comments about the dataset presented nor about the tentative age attribution which I find consistent also with the ice-stratigraphic evidence. I also agree with the authors that the summit area is not the likely source for these BRH tephra, as even if potentially buried beneath the ice filling the crater, the total lack of correlatable deposits on the summit crater rim makes it impossible for such young deposits to be originated in the summit region. I therefore agree that some lateral vent should be identified as the source and considering the young age I would expect to see the evidence of one or more hawaiian/strombolian edifice(s) to which the tephra may be correlated. Based on my personal experience may I suggest to consider the units ROL and SCC in Giordano et al 2012 as potential sources, both younger than 90ka but unfortunately not dated precisely. ROL is an extensive ropey basaltic lava field and SCC is a hawaiitic strombolian cone which both show no evidence of magma-ice interaction. The chemical characteristics and the eruption styles seem compatible, as well as the location, which is not far from the ice cliff where the BRH samples have been taken. I would recommend the authors to give a bit more space in the discussion to exploring where could the vent(s) be located along the Mt Melbourne flank and come up with some potential sources, as again the very young age of the tephra calls for their source identification

I hope these comments may be helpful

Guido Giordano

Reply: We agree with Reviewer #3 and we added some sentences in the Discussion section suggesting the possible correlation between our tephra and the scoria cone around the Mount Melbourne volcano.

**Author Comments:**

Dear Editor,

Please find below the reply to Editor's and reviewers' comments on the manuscript "Historical explosive activity of Mount Melbourne Volcanic Field (Antarctica) revealed by englacial tephra deposits" by Paola Del Carlo, Alessio Di Roberto, Giuseppe Re, Paul G. Albert, Victoria C. Smith, Gaetano Giudice, Graziano Larocca, Bianca Scateni and Andrea Cannata to be considered for publication on Bulletin of Volcanology. We have accepted the suggestions that we believe have improved the paper, so we would like to thank them for the revisions. We hope that we have fully addressed all the questions raised by the Reviewers. We also included in the ms the changes that were flagged on the annotated PDFs.

Best Regards

Di Roberto and co-authors

[Click here to view linked References](#)

1 **Historical explosive activity of Mount Melbourne Volcanic Field (Antarctica) revealed by**  
2 **englacial tephra deposits**

3  
4 Paola Del Carlo<sup>1</sup>, Alessio Di Roberto<sup>1\*</sup>, Giuseppe Re<sup>1</sup>, Paul G. Albert<sup>2</sup>, Victoria C. Smith<sup>3</sup>, Gaetano  
5 Giudice<sup>4</sup>, Graziano Larocca<sup>4</sup>, Bianca Scateni<sup>1,5</sup>, Andrea Cannata<sup>4,6</sup>

6  
7 (1) Istituto Nazionale di Geofisica e Vulcanologia, Sezione di Pisa, via C. Battisti 53, 56125 Pisa,  
8 Italy

9 (2) Department of Geography, Swansea University, Singleton Park, Swansea, SA2 8PP, UK

10 (3) Research Laboratory for Archaeology and the History of Art, 1 South Parks Road, University of  
11 Oxford, OX1 3TG, UK

12 (4) Istituto Nazionale di Geofisica e Vulcanologia, Osservatorio Etneo, Piazza Roma 2, 95125  
13 Catania, Italy

14 (5) Dipartimento di Scienze della Terra, Università di Pisa, 56126 Pisa, Italy

15 (6) Dipartimento di Scienze Biologiche, Geologiche e Ambientali, Università di Catania, Corso Italia  
16 57, 95125 Catania, Italy

17  
18 \*Corresponding author Alessio Di Roberto: [alessio.diroberto@ingv.it](mailto:alessio.diroberto@ingv.it)

19  
20 **Keywords:** Antarctica, Mount Melbourne Volcanic Field, Explosive eruptions, Englacial Tephra,  
21 Glass geochemistry, Historical eruptions

22  
23 **Abstract**

24 Five tephra layers named BRH1 to 5 have been sampled in an ice cliff located on the north-eastern  
25 flank of Mount Melbourne (northern Victoria Land, Antarctica). The texture, componentry,  
26 mineralogy and major- and trace-elements compositions of glass shards have been used to  
27 characterise these layers. These properties suggest that they are primary fall deposits produced from  
28 discrete eruptions that experienced varying degrees of magma/water interaction. The major- and  
29 trace-element glass shard analyses on single glass shards indicate that Mount Melbourne Volcanic  
30 Field is the source of these tephra layers and the geochemical diversity highlights that the eruptions  
31 were fed by compositionally diverse melts that are interpreted to be from a complex magma system  
32 with a mafic melt remobilizing more evolved trachy-andesitic to trachytic magma pockets.  
33 Geochemical compositions, along with textural and mineralogical data, have allowed correlations  
34 between two of the englacial tephra and distal cryptotephra from Mount Melbourne, recovered within

35 a marine sediment core in the Edisto Inlet (~280 km northeast of Mount Melbourne), and constrain  
36 the age of these englacial tephra layers to between the 3<sup>rd</sup> and the 4<sup>th</sup> centuries CE.

37 This work provides new evidence of the intense historical explosive activity of the Mount Melbourne  
38 Volcanic Field and better constrains the rates of volcanism in northern Victoria Land. These data  
39 grant new clues on the eruptive dynamics and tephra dispersal, and considerably expand the  
40 geochemical (major and trace elements) dataset available for the Mount Melbourne Volcanic Field.  
41 In the future, this will facilitate the precise identification of tephra layers from this volcanic source  
42 and will help define the temporal and spatial correlation between Antarctic records using tephra  
43 layers. Finally, this work also yields new valuable time-stratigraphic marker horizons for future  
44 dating, synchronisation and correlations of different paleoenvironmental and paleoclimatic records  
45 across large regions of Antarctica.

46

## 47 **1. Introduction**

48 Tephra in Antarctic ice records (ice cores or blue-ice) provide important sources of data for evaluating  
49 the history and evolution of Antarctic explosive volcanism. The typical absence of pyroclastic  
50 deposits at proximal locations on the flanks of the volcanoes, due to high rates of post-depositional  
51 erosion and/or remobilization and also (mainly) the extensive cover of snow and ice obscuring  
52 deposits on the volcanic centres, limit the reconstruction of past volcanic eruptions, including their  
53 timing, scale, and impact on the environment. This gap in knowledge can be overcome by the study  
54 of tephra and cryptotephra (not visible, highly disseminated, fine-grained tephra) at medial to distal  
55 sites, which are preserved and remain unaltered within the snow, transformed into glacial ice upon  
56 burial (Smellie 1999; Harpel et al. 2008; Iverson et al. 2017). In polar regions, and particularly in  
57 Antarctica, tephrochronological studies in ice cores and blue-ice records have been well developed  
58 over recent decades (e.g. Narcisi et al. 2005; Kurbatov et al. 2006; Curzio et al. 2008; Iverson et al.  
59 2014; Wolff et al. 2010; Narcisi et al. 2012; Severi et al. 2012; Kim et al. 2020; Nardin et al. 2021).  
60 Along with tephra included in marine sediment sequences (Hillenbrand et al. 2008; Del Carlo et al.  
61 2015; Di Roberto et al. 2019; 2020; 2021a; 2021b; 2023), tephra deposits in englacial sequences can  
62 help improve near-vent eruption records, in terms of both frequency/chronology of explosive  
63 volcanism, and magma chemical evolution through time, whilst facilitating advancements in the  
64 dating, correlating, and synchronising high-resolution climate and atmospheric composition records  
65 through the Late Quaternary (Narcisi and Petit 2021). In addition, tephrochronological correlations  
66 between different archives (e.g., ice and marine records), located at proximal and distal sites from an  
67 eruptive source, are greatly enhanced once a numerical age is obtained for tephra. Specifically, the



68 correlation of two tephra layers allows the age-transfer from one site to another by the simple use of  
69 stratigraphy, heightening tephrochronology to an age-equivalent dating method (Lowe 2011).

70 Mount Melbourne is an active volcano in northern Victoria Land, Antarctica, and future activity on  
71 the volcano would pose a significant tephra fall risk to nearby scientific stations e.g. Mario Zucchelli  
72 Station (Italian), Jang Bogo (Korea), Gondwana (Germany), and the new China Antarctic research  
73 base (Figure 1a), as well as to Austral hemisphere air traffic. Therefore, a good knowledge of the  
74 recent volcanic activity of this volcano is important to better evaluate the possible volcanic hazards  
75 (Geyer 2021).

76 The earliest investigations on Mount Melbourne began at the end of the 1960s whereas the first  
77 geophysical observations started in 1988 by Italian National Antarctic Research Program (PNRA);  
78 no eruptive activity has been observed at this volcano. The age of the most recent eruption is proposed  
79 by Lyon (1986) who performed the stable isotope analysis of two snow profiles sampled on Mount  
80 Melbourne at ca. 2000 m of altitude and on the Campbell Glacier obtaining snow accumulation rates  
81 of 0.5-2.2 m/a. Using these data, the author derived the age of englacial ash layers outcropping in an  
82 ice cliff at ca. 1200 m of altitude on the western slope of Mount Melbourne and photographed in 1965  
83 by Adamson and Cavaney (1967). They roughly estimated the depth of snow from the surface to the  
84 first major ash layer to be between 29 and 36 m and, considering an accumulation rate of  $0.5 \pm 0.16$   
85 m/a, the last major eruption should have occurred between 1862 and 1922 AD. Although this method  
86 has several limitations (e.g. the lack of direct measurement of the snow thickness, or the detailed  
87 study of snow profile aimed at identifying possible hiatus or erosion surfaces) it does provide an  
88 estimate of the age of the latest eruptive activity of Mount Melbourne. Unfortunately, the englacial  
89 tephra layers described in Lyon (1986) and Adamson and Cavaney (1967) have never been sampled  
90 nor characterised in their textural and geochemical features because the outcrop did not allow safe  
91 sampling.

92 During the 2017 austral summer, the ICE-VOLC project (PNRA) facilitated new geological surveys  
93 around Mount Melbourne which revealed the occurrence of multiple englacial volcanic ash layers in  
94 an ice cliff located on the northeast flank of the volcano at ca. 800 m of altitude, very close to Baker  
95 Rock location (Gambino et al. 2021; Figure 1). The better accessibility of the outcrop allowed the  
96 sampling of tephra and the measurements of the thickness between the different ash layers.

97 In this paper, we present data on the texture, mineral phases, and major- and trace-element  
98 geochemical data performed on single glass shards analysed via Electron Probe Microanalysis  
99 (EMPA) and Laser Ablation Inductively Coupled Plasma Mass Spectrometry (LA-ICP-MS) of five  
100 englacial tephra layers sampled for the first time from the north-eastern flank of Mount Melbourne.  
101 Geochemical data indicate that the tephra layers derive from Mount Melbourne explosive activity.

102 The texture of the particles and their morphological features were important for clues to the style of  
103 the eruptions and fragmentation mechanisms. In addition, geochemical fingerprints of englacial  
104 tephra have allowed their correlations and dating with cryptotephra layers recently found in marine  
105 sediments in Edisto Inlet near Cape Hallett (Di Roberto et al. 2023), highlighting that Mount  
106 Melbourne has been very active during historical times.

107

## 108 **2. Geological setting**

109 Mount Melbourne stands as a 2732-m high stratovolcano with a basal diameter of about 21-24 km on  
110 the coast of northern Victoria Land, between Wood Bay and Terra Nova Bay, in Antarctica (Figure  
111 1b). The Mount Melbourne volcano also includes several parasitic cones and secondary vents located  
112 on the flank of the main edifice (Smellie et al. 2023). The main volcano edifice shows a gentle shape  
113 with undissected flanks, apart from a possible slump scar on the east side (Giordano et al. 2012), and  
114 a well-formed ice-filled crater ca. 700 m in diameter that Armienti et al. (1991) interpreted as a  
115 summit caldera. It is largely covered by snow and ice except for the summit region where rock  
116 outcrops extend downslope on the east side to ca. 1800 m. The Mount Melbourne Volcanic Field  
117 (MMVF), together with The Pleiades, Mount Overlord, Mount Rittmann, and the Malta Plateau  
118 volcanoes, is part of the Melbourne Volcanic Province within the McMurdo Volcanic Group (Smellie  
119 and Rocchi 2021). A synthesis of MMVF volcanic history has been reported by Giordano et al. (2012)  
120 and Smellie et al. (2023) based on stratigraphic and volcanological studies, geochemical data, and  
121 age determinations. According to recent updates based on radioisotopic ages, the MMVF volcanism  
122 began in the Late Miocene (c. 12.5 Ma for centres in the north by Tinker Glacier) but developed  
123 mainly from the Pliocene (c. 4 Ma; Smellie et al. 2023) particularly after c. 3 million years ago  
124 (Rocchi and Smellie 2021 and references therein). The activity can be subdivided into different  
125 evolution stages: i) the older Cape Washington shield volcano (Late Miocene-Late Pliocene), ii) the  
126 Random Hills Period (Lower-Middle Pleistocene), iii) the Shield Nunatak Period (Middle  
127 Pleistocene) and iv) the Mount Melbourne Period (Upper Pleistocene-present; Giordano et al. 2012;  
128 Smellie et al. 2023).

129 The oldest deposit that can be linked directly to an eruption of the Mount Melbourne stratovolcano,  
130 re-dated as 115 ka by Smellie et al. (2023) at Edmonson Point, is a trachytic ignimbrite. This was  
131 emplaced during a large Plinian eruption and indicates the formation of a crustal magma chamber  
132 during the recent Mount Melbourne stage (Giordano et al. 2012). Subsequently, the Adelie Penguin  
133 Rookery lava field succession was produced comprising alkali basaltic, hawaiitic, and subordinate  
134 benmoreitic lavas, scoria cones and spatter cones that are dated at  $90.7 \pm 19.0$  ka. (Giordano et al.  
135 2012).

136 Evidence of more recent activity, based on tephrostratigraphic analysis and  $^{40}\text{Ar}$ - $^{39}\text{Ar}$  dating of  
137 proximal pyroclastic sequence exposed on the Mount Melbourne summit, indicates there were at least  
138 four Strombolian or Vulcanian style to sub-Plinian/Plinian eruptions during the Late Pleistocene to  
139 Holocene (Del Carlo et al. 2022). The most intense of these eruptions was a sub-Plinian to Plinian  
140 eruption that yielded an age  $<17.8$  ka ( $13.5\pm 4.3$  ka). Furthermore, three trachytic cryptotephra with  
141 glass compositions similar to Mount Melbourne products were found intercalated in marine sediments  
142 of Edisto Inlet, near Cape Hallett (Di Roberto et al. 2023). These cryptotephra layers were interpreted  
143 as derived from historic explosive eruptions of Mount Melbourne that occurred between 1615 cal.  
144 yrs BP and 1677 cal. yrs BP, i.e. between the 3<sup>rd</sup> and 4<sup>th</sup> centuries CE (Di Roberto et al. 2023).  
145 Presently, the Mount Melbourne volcano is quiescent with thermal anomalies, including noticeable  
146 steaming or fumarolic activity both in the crater and on the north-western side of the volcano. These  
147 emissions of steam and volcanic gas have produced several ice towers and a complex network of ice  
148 caves, as recently reported after geochemical surveys in the frame of the ICE-VOLC project  
149 (Gambino et al. 2021).

150

## 151 **2. Material and Methods**

152 During the XXXII Italian Antarctic Expedition in 2017, the area surrounding Mount Melbourne was  
153 aerially surveyed by helicopter flights. A series of dark, sub-horizontal englacial tephra layers were  
154 found exposed along a ca. 50-metres-high ice cliff located on the north-eastern flank of the volcano  
155 at about 800 m of altitude close to Baker Rock (74.24096 S, 164.72032 E; red star in Figure 1). Five  
156 sub-horizontal tephra layers, named BRH1 to 5 (from the top to the bottom), were distinguished and  
157 sampled by the Italian alpine climbing guides (Figure 2). Tephra layers are between 10 and 20  
158 centimetres thick and are each separated by 1.5 to 7.5 metres of ice (Figure 2). Each sample is a “bulk”  
159 sample of the tephra layer and represents the whole unit; unfortunately, due to the extreme sampling  
160 conditions, it was not possible to sub-sample different stratigraphic heights within each unit. The  
161 tephra samples were recovered still embedded in the ice, which was then melted to recover the clastic  
162 fraction.

163 Sample preparation was carried out at laboratories of Istituto Nazionale di Geofisica e Vulcanologia,  
164 Sezione di Pisa (INGV-Pisa). Samples were washed with deionized water in an ultrasonic bath to  
165 remove impurities, dried at 60°C, mounted with epoxy resin in 1-inch stubs, polished, and prepared  
166 for textural and geochemical analyses. Textures, components, and mineral assemblages of each tephra  
167 were studied with an optical microscope and a scanning electron microscope (SEM) Zeiss EVO MA  
168 and images of 3D silhouettes and 2D cross-sections have been collected in secondary (SE) and back-  
169 scattered (BSE) electrons mode, respectively. The major and minor element glass composition of

170 samples was determined using a JEOL 8600 wavelength-dispersive electron microprobe equipped  
171 with four spectrometers at the Research Laboratory for Archaeology and the History of Art, the  
172 University of Oxford (operating conditions: 15 kV accelerating voltage, 6 nA beam current and a  
173 beam diameter of 10  $\mu\text{m}$ ). The JEOL 8600 electron microprobe was calibrated with a suite of  
174 appropriate mineral standards; peak count times were 30 s for all elements except Mn (40s), Na (12s),  
175 Cl (50s), and P (60s). The PAP absorption correction method was used for quantification. Reference  
176 glasses from the Max Planck Institute (MPI-DING suite; Jochum et al., 2006) bracketing the possible  
177 chemistries were also analysed. These included felsic [ATHO-G (rhyolite)], through intermediate  
178 [StHs6/80-G (andesite)] to mafic [GOR132-G (komatiite)] glasses. All glass data have been  
179 normalised to 100% for comparative purposes. Uncertainties are typically  $< \pm 0.8\%$  RSD for Si;  $\sim \pm$   
180  $5\%$  for most other major elements, except for the low abundance elements for instance Ti ( $\sim \pm 7\%$ )  
181 and Mn ( $\sim \pm 30\%$ ).

182 Trace element analysis of volcanic glass was performed using an Agilent 8900 triple quadrupole ICP-  
183 MS (ICP QQQ) coupled to a Resonetics 193 nm ArF excimer laser-ablation in the Department of  
184 Earth Sciences, Royal Holloway, University of London. Full analytical procedures used are reported  
185 in Tomlinson et al. (2010). Spot sizes 20 and 25  $\mu\text{m}$  were used depending on the vesicularity, crystal  
186 content, and ultimately the size of available glass surfaces. The repetition rate was 5 Hz, with a count  
187 time of 40 s on the sample, and 40 s on the gas blank to allow the subtraction of the background  
188 signal. Blocks of eight or nine glass shards and one MPI-DING reference glass were bracketed by the  
189 NIST612 glass calibration standard (GeoREM 11/2006). In addition, MPI-DING reference glasses  
190 were used to monitor analytical accuracy (Jochum et al. 2005). The internal standard applied was  $^{29}\text{Si}$   
191 (determined by the EMPA analysis). Where individual shards were arranged into a grid formation  
192 across an epoxy mount they are given a unique row (A, B, C) and shard number (1, 2, 3). In these  
193 instances, the grain-specific  $^{29}\text{Si}$  content was applied as the internal standard. Where tephra samples  
194 were mounted in epoxy mounts without shard mapping, average  $^{29}\text{Si}$  contents for the appropriate  
195 compositional groupings within the tephra deposit, determined based on EMPA analysis, were  
196 applied as the internal standard to the individual glass shards ablated. Internal standard values applied  
197 to individual shard ablations are provided in the Supplementary Information. LA-ICP-MS data  
198 reduction was performed in Microsoft Excel. Accuracies of LA-ICP-MS analyses of MPI-DING glass  
199 standards ATHO-G and StHs6/80-G were typically  $< 5\%$ . Full glass datasets and MPI-DING standard  
200 glass analyses are provided in Supplemental Information.

201

## 202 **3. Results**

### 203 *3.1 Texture and components of tephra layers*

204 BRH samples are similar in terms of components, comprising a range of clasts with different textures  
205 ranging from dense to highly-vesicular and glassy to microlite-rich (Figures 3 and 4a-e). The  
206 morphology of juvenile clasts ranges from equant with rounded vesicles (Figure 4f) to fluidal with  
207 elongated tubular vesicles (Figures 4g, h). Dense poorly vesicular juveniles display features such as  
208 stepped surfaces and hackle lines, quenching cracks and pitted surfaces (Figures 4l, m), similar to the  
209 glassy shards that range from blocky to platy (Figures 4i, n).

210 Overall, the grain-size, scarcity of non-volcanic detrital material and unabraded pristine shapes of the  
211 clasts indicate that these decimetre-thick layers are emplaced as primary fallout deposits. Extremely  
212 fragile particles such as glass fibres (Pele's hair) survived, and the external morphology of vesicular  
213 particles preserves pristine elements like fragile glass fibres, glass tips, spiny glass edges (Figures 3  
214 and 4), or glass coatings around magmatic crystals. Particles do not exhibit surficial alteration textures  
215 due to weathering, surface abrasion, or rounding. Lithic or detrital fragments are also scarce. All these  
216 features along with the geochemical fingerprints (see next paragraph) indicate very minor or no  
217 aeolian remobilization, re-sedimentation, or other transport after the deposition from the volcanic  
218 plume. Moreover, the layers occur close to the surface of the ice cover and well above the glacier  
219 bed, hence are unlikely to be glacier bedload brought to the surface by shearing.

220 As mentioned in the Material and Methods section, the studied material comprises "bulk" samples of  
221 each tephra layer. Possible internal stratifications resulting from variations in eruptive style, energy,  
222 dynamics, magma reflected by changes in the glass composition, grain size, componentry, etc. were  
223 lost.

224  
225 BRH1 tephra is the uppermost tephra exposed at the top of the ice cliff. It is made of coarse to very  
226 fine ash (Figure 4a) and comprises two discrete particle populations differing in colour, shape, and  
227 texture. The first population, which is the more abundant, consists of shiny, black to dark brown,  
228 vesicular glassy clasts (Figures 3a and g) with spiny to fluidal shapes (Figure 3d), volcanic glass  
229 fibres, and glass droplets (Pele's hair and tears; Figure 3c) and minor amounts of grey, dense and  
230 blocky clasts (Figure 3b). Often particles with fluidal shapes are bounded by sharp-planar breakage  
231 surfaces (Figure 3g). Fluidal clasts (Figure 3a) are usually glassy aphyric to microlite-poor, poorly to  
232 moderately vesicular with spherical vesicles. Blocky clasts (Figure 3b) are almost non-vesicular to  
233 very poorly vesicular with abundant microlites and microphenocrysts of andesine plagioclase (up to  
234 60  $\mu\text{m}$ ), Fe-augite clinopyroxene (up to 30  $\mu\text{m}$ ), olivine ( $\sim\text{Fo}_{45}$ ; up to 10  $\mu\text{m}$ ), Fe-Ti oxides (up to 10  
235  $\mu\text{m}$ ), and rare apatite (up to 10  $\mu\text{m}$ ). Also, crystals (up to ca. 250  $\mu\text{m}$ ) of plagioclase, olivine and  
236 clinopyroxene occur coated in a dark glass.

237 The second particle population represents approximately 30% of the sample and has a finer grain size  
238 (fine ash). Particles comprise white to pale yellow, highly vesicular pumice fragments, and nearly  
239 transparent glass shards (Figure 4a). Pumice fragments often show elongated to tubular vesicles  
240 (Figure 3f), and bear within an aphyric groundmass abundant labradorite plagioclase (up to 80  $\mu\text{m}$ )  
241 and olivine ( $\sim\text{Fo}_{75}$ ; up to 30  $\mu\text{m}$ ) with rare Mg-augite clinopyroxene (up to 20  $\mu\text{m}$ ) and Mg-chromite  
242 spinel (up to 10  $\mu\text{m}$ ). Lithic clasts are scarce in BRH1 tephra and consist of reddish or altered volcanic  
243 rocks (Figure 3e).

244

245 BRH2 tephra is a poorly sorted lapilli (up to 4 mm) and ash (Figure 4b) layer. It is predominantly  
246 composed of black/dark brown, shiny, vesicular glass fragments with spiny and fluidal shapes again  
247 often bounded by sharp-planar breakage surfaces (Figure 3d), Pele's hair and tears, highly vesicular  
248 fragments, and grey dense, blocky clasts. Fluidal clasts (Figure 4b) have glassy groundmass with  
249 spherical to elliptical vesicles and contain abundant microlites of andesine to oligoclase plagioclase  
250 (up to 50  $\mu\text{m}$ ), Fe-rich olivine ( $\sim\text{Fo}_{35}$ ; up to 15  $\mu\text{m}$ ), Fe-augite clinopyroxene (up to 30  $\mu\text{m}$ ), and Fe-  
251 Ti oxides ( $\sim 10 \mu\text{m}$ ). Grey dense and blocky clasts (Figure 4b) are porphyritic with microphenocrysts  
252 of oligoclase to anorthoclase feldspar, Fe-augite, and Fe-Ti oxides within a glassy to microcrystalline  
253 groundmass. Tubular pumice fragments and bubble wall glass shards are abundant in the fine-grained,  
254 fine ash-sized portion of the deposit. Pumices have a glassy groundmass sometimes with acicular  
255 microlites of anorthitic feldspar. Scarce lithic clasts consist of reddish, altered volcanic rocks and  
256 intrusive rock fragments. Loose crystals of anorthoclase, clinopyroxene and fayalite are abundant.

257

258 BRH3 tephra (Figure 4c) is fine ash, with scarce scoriaceous fine lapilli, made of black to dark brown,  
259 shiny, poorly to moderately vesicular, fluidal glass particles (Figure 4g) and grey, blocky fragments  
260 (Figure 4n). Dark glass-coated crystals of plagioclase, clinopyroxene, and olivine are also abundant.  
261 Fluidal clasts are moderately vesicular, mainly with rounded tubular vesicles (Figure 4g), and have  
262 glassy groundmass with phenocrysts of oligoclase plagioclase (up to 250  $\mu\text{m}$ ) and Fe-augite  
263 clinopyroxene (up to 350  $\mu\text{m}$ ); accessory minerals are anorthoclase feldspar ( $\sim 90 \mu\text{m}$ ), olivine ( $\sim\text{Fo}_{20}$ ;  
264  $\sim 25 \mu\text{m}$ ), Fe-Ti oxides ( $\sim 15 \mu\text{m}$ ) and apatite ( $\sim 45 \mu\text{m}$ ). Blocky fragments are poorly vesicular with  
265 abundant microlites of plagioclase, clinopyroxene, olivine, and Fe-Ti oxides. Pale yellow to white  
266 fibrous pumiceous clasts are also abundant in BRH3 tephra. Pumice fragments are mostly aphyric,  
267 with rare microphenocrysts of plagioclase and Fe-Ti oxides within a glassy highly vesicular  
268 groundmass with elongated vesicles. Lithic clasts consist of red, oxidised lava fragments, and altered  
269 tuffaceous rock fragments.

270

271 BRH4 tephra (Figure 4d) is a very poorly sorted lapilli (up to 2 mm) to very fine ash layer. The sample  
272 is almost completely formed by black, shiny, spiny glass fragments and Pele's hair and tears, grey,  
273 dense and blocky clasts, and glass fragments (Figure 4i). Golden-coloured, moderately vesicular  
274 glassy fragments are also present. Fluidal clasts (Figure 4h) and golden vesicular fragments have  
275 porphyritic texture, with microphenocrysts of andesine plagioclase (~ 100  $\mu\text{m}$ ), olivine (~ $\text{Fo}_{50}$ ; ~20  
276  $\mu\text{m}$ ), Fe-Ti oxides (~10  $\mu\text{m}$ ), within a glassy groundmass with rounded vesicles. The grey blocky  
277 particles (Figure 4d) are highly porphyritic with abundant microphenocrysts of oligoclase plagioclase  
278 (~80  $\mu\text{m}$ ), Fe-Ti oxides (~45  $\mu\text{m}$ ) and olivine (~ $\text{Fo}_{45}$ ; ~40  $\mu\text{m}$ ), and subordinate anorthoclase/sanidine  
279 feldspar (~ 30  $\mu\text{m}$ ), Fe-augite clinopyroxene (~40  $\mu\text{m}$ ) and apatite (~25  $\mu\text{m}$ ), within a microlite-rich  
280 glassy groundmass. Many clasts show truncated shapes. Loose crystals of plagioclase, clinopyroxene,  
281 and olivine are abundant. Lithic clasts comprise lava and tuff fragments. A minor quantity of whitish,  
282 spongy pumice clasts is also present in the fine ash-sized fraction of the deposit. Pumice particles are  
283 aphyric and often present altered groundmass.

284  
285 BRH5 tephra (Figure 4e) is a very poorly sorted fine lapilli (up to 2 mm) to a fine ash layer. It  
286 comprises dark brown to black and shiny, vesicular glass fragments with spiny (Figure 4i), fluidal,  
287 and blocky shapes, glass shards, and a few grey dense blocky clasts. Dense clasts are poorly vesicular,  
288 with spaced rounded to amoeboid vesicles, and porphyritic, with abundant microphenocrysts of  
289 labradorite plagioclase (up to 140  $\mu\text{m}$ ), olivine (~ $\text{Fo}_{60}$ ; ~50  $\mu\text{m}$ ), Fe-Ti oxides (~30  $\mu\text{m}$ ), within a  
290 glassy groundmass with abundant microlites of plagioclase, Fe-rich olivine, Fe-augite clinopyroxene  
291 (up to 15  $\mu\text{m}$ ) and rare apatite (~10  $\mu\text{m}$ ). Clear to light grey pumice fragments are also abundant (ca.  
292 20%). Pumices are highly vesicular with rounded and non-collapsed to tubular and stretched vesicles  
293 (Figure 4e), bearing rare microphenocrysts of acicular labradorite to andesine plagioclase (up to 200  
294  $\mu\text{m}$ ) and Fe-rich olivine (~25  $\mu\text{m}$ ) within a glassy groundmass with rare microlites of plagioclase,  
295 clinopyroxene olivine and Fe-Ti oxides. Some pumice fragments, which have coarse amoeboid and  
296 collapsed vesicles, have domains with glassy groundmass and domains with microcrystalline ones  
297 (Figure 4e). Loose crystals of plagioclase, clinopyroxene, and olivine are also present. Lithic clasts  
298 include reddish to pinkish, oxidised pumices and rare fragments of granitoid rocks.

299

300

### 301 *3.2 Major, minor and trace element glass geochemistry*

302 Representative major, minor and trace element glass chemistry from the BRH 1 to 5 tephra layers are  
303 provided in Table 1, while the full datasets are provided in the Supplementary Information.

304 The tephra layers analysed (BRH1 to 5) display more than one compositional component, consistent  
305 with their variable textures and componentry, consequently, compositions range from basalts, through  
306 basaltic trachy-andesites and trachy-andesites to more evolved trachytes (Figure 5a). Glasses are all  
307 characterised by high analytical totals suggesting a very minor amount of post-depositional alteration  
308 and/or reworking.

309 BRH1 to 5 volcanic glasses predominantly straddle the High-K calc-alkaline and Shoshonitic  
310 boundary, with the more evolved trachytic end-members residing more clearly within the shoshonitic  
311 field (Figure 5b). The absence of negative anomalies at Nb and Ta in the mantle-normalised trace  
312 element profiles of the BRH1 to 5 volcanic glasses is clearly consistent with Antarctic alkaline  
313 regional volcanism within the West Antarctic Rift System (Panter, 2021), and the absence of  
314 significant crustal involvement in magma genesis (Figure 6). As is to be expected, overall levels of  
315 incompatible trace element enrichment are significantly greater in the trachytic end-member glasses  
316 of the tephra units relative to their more mafic components (Figure 7). Light Rare Earth Elements  
317 (LREE) are enriched relative to the Heavy Rare Earth Elements (HREE), and the relative level of  
318 enrichment remains fairly constant spanning from the basalts through to the trachytes ( $La/Yb_N \sim 13-$   
319  $14$ ). Trachytic end-member glasses display depletions in Ba, Sr and Eu consistent with feldspar  
320 fractionation, with these anomalies absent in the more primitive (basaltic) glasses. Owing to the  
321 significant heterogeneity of the BRH tephra layers we describe the chemical signature of dominant  
322 chemical clusters or components, and therefore rare outlying analyses are not described in detail.

323

324 BRH1 ( $n=18/24$ ), BRH2 ( $n=13/33$ ) and BRH5 ( $n=15/30$ ) tephra layers all contain a significant mafic  
325 glass component associated with the black glassy and fluidal particles, which display a relatively  
326 narrow compositional range within the basalt compositional field (44.5 to 46.0 wt.%  $SiO_2$ , and 3.9 to  
327 5.3  $Na_2O + K_2O$ ), with minor overlap into the basanite field (Figure 5a). More noticeable  
328 compositional variability in these basalts is observed in other major oxides, for instance with 7.3-4.7  
329 wt.%  $MgO$ , 14-12 wt.%  $FeO_t$ , 12.1-9.7 wt.%  $CaO$  and 5.0-3.3 wt.%  $TiO_2$ , where this variability is  
330 consistent between the basalts of all three layers (Figure 5). Tephra layer BRH3 also contains  
331 dark glassy material entirely consistent with the basaltic glasses of the BRH1, 2 and 5 tephra layers,  
332 however, these compositions are not as well represented in the chemical analysis of the tephra  
333 ( $n=10/74$ ), which are dominated by a trachytic end-member (Figure 5a).

334 The incompatible trace elements content of these basaltic glasses, predominantly those successfully  
335 analysed from the BRH1 and BRH5 layers, reveal significant variability for instance 128-236 ppm  
336 Zr, 15.3-28.0 ppm Y and 2.6-4.7 ppm Th (Figure 7). Ratios of High Field Strength Elements (HFSE)  
337 vs. Th in these basaltic glasses show some variability (e.g.,  $Zr/Th = 46.3-54.3$ ;  $Nb/Th = 14.2-15.5$ ;



338 Y/Th = 5.6-6.6). These basaltic glasses display high LREE relative to the HREE where  $\text{La/Yb}_N =$   
339  $13.0 \pm 0.9$  (1 s.d). Despite the overall variability within the basaltic glasses analysed they are  
340 chemically indistinguishable through the successive tephra layers, suggesting a common magmatic  
341 source.

342

343 BRH1 glasses, consistent with the observed componentry (see above), are chemically bimodal, in  
344 addition to the dominant dark glassy basaltic component already described, the tephra layer also  
345 contains a homogeneous secondary trachytic component ( $\text{SiO}_2 = 65.2 \pm 0.1$  wt. % and  $\text{Na}_2\text{O} + \text{K}_2\text{O} =$   
346  $10.78 \pm 0.1$  wt. %;  $n=5/23$ ). The incompatible trace elements content of these trachytic glasses ( $n=4$ )  
347 are relatively homogeneous, for instance,  $676 \pm 40$  ppm Zr,  $54 \pm 4$  ppm Y, and  $21 \pm 2$  ppm Th, whilst  
348 these levels of enrichment far exceed those of the dominant basaltic end-member (Figure 7). Ratios  
349 of HFSE vs. Th become significantly lower ( $\text{Zr/Th} = 33.0 \pm 1.3$ ;  $\text{Nb/Th} = 8.1 \pm 0.5$ ;  $\text{Y/Th} = 2.6 \pm 0.1$   
350 [1 s.d]) than those of the basaltic component (Figure 7). These evolved trachytic glasses display  
351 particularly strong negative Sr anomalies ( $\text{Sr/Pr}_N = 0.09 \pm 0.003$ ), but also less pronounced anomalies  
352 in Ba and Eu (Figure 6).

353

354 Overall, BRH2 glasses cover a wide compositional range, consistent with the mixed componentry  
355 (Section 3.1). As with BRH1, the basaltic glass forms a significant component (1) of BRH2. In  
356 addition, at least two other compositional components or clusters are observed in BRH2, which plot  
357 along an evolutionary trend that extends toward the highly evolved trachytes, similar to the overlying  
358 BRH1 tephra ( $\sim 65$  wt. %  $\text{SiO}_2$ ). BRH2 glass component 2 straddles the boundary between the basaltic  
359 trachy-andesite to trachy-andesite compositional fields with between 54.5-56.5 wt.%  $\text{SiO}_2$  and where  
360  $\text{Na}_2\text{O} + \text{K}_2\text{O} = 6.9-8.4$  wt. % (Figure 5a). BRH2 component 3 glasses are more variable and evolved  
361 than component 2 predominantly clustering at the boundary between the trachy-andesite and trachytic  
362 field, albeit with a small number of analyses extending towards the more evolved trachytic  
363 endmember of BRH1 (Figure 5a).

364 Trace element analysis of BRH2 component 2 (basaltic trachy-andesite/trachy-andesite) glasses  
365 was unsuccessful due to the presence of microlites, but trace elements analyses were acquired for  
366 glass component 3. The trachy-andesites through to trachytes, are equally heterogeneous at the trace  
367 elements level, with 388-720 ppm Zr, 10.0-21.9 ppm Th. The glasses show depletions in Sr ( $\text{Sr/Pr}_N$   
368  $= 0.30 \pm 0.1$  [1 s.d]) and Eu, however, these are not as pronounced as those observed in the more  
369 evolved trachytes of BRH1 (Figure 6). HFSE ratios to Th in these glasses remain constant despite the  
370 variability in absolute concentrations ( $\text{Zr/Th} 33.6 \pm 1.6$ ;  $\text{Nb/Th} = 8.4 \pm 0.9$ ;  $\text{Y/Th} = 3.1 \pm 0.2$  [1 s.d]).  
371 The Zr/Th and Nb/Th ratios are broadly consistent with the more evolved (trachytic) glasses of the

372 overlying BRH1, but again are significantly lower than those of the basaltic glasses in this tephra (and  
373 BRH1; Figure 7).

374

375 In addition to a basaltic component, the BRH3 tephra has a minor population of intermediate glasses  
376 which straddle the basaltic trachy-andesite to trachy-andesite compositional fields, similar to  
377 component 2 of the overlying tephra BRH2 (Figure 5a). A significant component of BRH3 analyses  
378 ( $n = 51/73$ ) lies firmly in the trachytic compositional field, with 62.1-67.2 wt. %  $\text{SiO}_2$  and 8.8-10.6  
379 wt. %  $\text{Na}_2\text{O} + \text{K}_2\text{O}$  and relate to the pumiceous material within this tephra layer. Within these variable  
380 trachytic compositions, a dominant cluster of shoshonitic glasses is clearly recognized at ~66 wt. %  
381  $\text{SiO}_2$ , and ~4.9  $\text{K}_2\text{O}$  (Figure 5b), where  $\text{Na}_2\text{O}$  is  $> \text{K}_2\text{O}$  ( $\text{K}_2\text{O}/\text{Na}_2\text{O} = 0.9$ ). These most evolved  
382 trachytes ( $n=16$ ) are extremely enriched in incompatible trace elements for instance 613-728 ppm Zr  
383 and 18.3-22.1 ppm Th. HFSE ratios vs. Th in these trachytic glasses remain constant where  $\text{Zr}/\text{Th} =$   
384  $33.0 \pm 0.8$ ,  $\text{Nb}/\text{Th} = 7.5 \pm 0.3$  and  $\text{Y}/\text{Th} = 2.5 \pm 0.1$  (Figure 7). They also display depletions in Ba, Sr  
385 ( $\text{Sr}/\text{Pr}_\text{N} = 0.10 \pm 0.01$ ) and Eu (Figure 6).

386

387 The glass compositions of BRH4 are heterogeneous, largely bimodal, with some glasses extending  
388 between the two dominant end-members. The least evolved glass component plots in the basaltic  
389 trachy-andesite compositional field ( $\text{SiO}_2 = 53.8\text{-}55.7$  wt. %  $\text{SiO}_2$ ,  $\text{Na}_2\text{O} + \text{K}_2\text{O} = 7.0\text{-}8.3$ ), whilst  
390 straddling the boundary with trachy-andesites (Figure 5a). The more evolved end-member is  
391 characterised by slightly more variable trachytic glass compositions with 62.6-66.5 wt.%  $\text{SiO}_2$  and  
392 9.1-10.5 wt.%  $\text{Na}_2\text{O} + \text{K}_2\text{O}$  (Figure 5a) and these relate to the pumice component of the deposit. The  
393 basaltic trachy-andesitic glasses ( $n = 5$ ) have some incompatible trace elements variability, for  
394 instance, 400-449 ppm Zr and 11.3-12.3 ppm Th (Figure 7). The HFSE ratios in these glasses are  
395 constant ( $36.7 \pm 0.2$   $\text{Zr}/\text{Th}$ ;  $9.6 \pm 0.1$   $\text{Nb}/\text{Th}$  and  $4.0 \pm 0.02$   $\text{Y}/\text{Th}$  [1 s.d]), whilst they show a small  
396 anomaly in Sr ( $\text{Sr}/\text{Pr}_\text{N} = 0.4 \pm 0.1$  [1 s.d]). The trachytic end-member glasses ( $n = 5$ ) are more enriched  
397 in incompatible elements than the basaltic trachy-andesites (Figure 7), and show considerable  
398 variability for instance 472-604 ppm Zr and 13.8-17.2 ppm Th. These trachytic glasses display  
399 constant HFSE ratios (e.g.,  $34.7 \pm 1.0$   $\text{Zr}/\text{Th}$ ,  $8.2 \pm 0.4$   $\text{Nb}/\text{Th}$  and  $2.8 \pm 0.3$   $\text{Y}/\text{Th}$ ), but are slightly  
400 lower than those of the basaltic trachy-andesites. The trachytic glasses display a greater depletion in  
401 Sr ( $\text{Sr}/\text{Pr}_\text{N} = 0.3 \pm 0.1$ ), along with additional depletions in Ba and Eu in contrast to the basaltic trachy-  
402 andesites (Figure 6). However, the removal of Sr from the melt composition of BRH4 is not as  
403 significant as for some of the more evolved trachytic glasses observed in the overlying tephra deposits  
404 (e.g., BRH1, BRH3; Figure 6).

405

406 Compositionally the BRH5 tephra layer is largely bi-modal, with some very minor evidence of  
407 intermediate glass compositions spanning an evolutionary trend between the two end-members,  
408 which are characterised by basaltic and trachytic glass populations (Figure 5a). The basaltic  
409 component is entirely consistent with those observed and described (above) from the BRH1, BRH2,  
410 and BRH3 tephra layers (Figures 5, 6 and 7). Whilst the trachytic end-member glasses are variable,  
411 they remain consistent with both dominant trachytic components of BRH1 and BRH3, where SiO<sub>2</sub>  
412 content of ~64.9 wt. % and ~66.8 wt. % SiO<sub>2</sub> respectively are observed (Figure 5a). The incompatible  
413 trace elements content of the BRH5 trachytic endmember ( $n = 5$ ) glasses are homogeneous with  $737$   
414  $\pm 30$  ppm Zr and  $23 \pm 1$  ppm Th. The levels of enrichment in some of these trachytic glasses extend  
415 to the highest observed throughout this englacial succession (Figure 7). Furthermore, strong  
416 depletions in Ba, Sr ( $\text{Sr}/\text{Pr}_N = 0.09 \pm 0.01$  [1 s.d]) and Eu are observed in these glasses (Figure 6).  
417 HFSE ratios to Th are constant ( $32.0 \pm 0.3$  Zr/Th,  $7.3 \pm 0.2$  Nb/Th,  $2.5 \pm 0.1$  Y/Th [1 s.d]) and are  
418 entirely consistent with the most evolved trachytic products seen in the BRH1 and BRH3 layers.

419

## 420 **4. Discussion**

421

### 422 *4.1 Volcanic source and proximal-distal correlation*

423 Major and trace elements glass compositions data show a strong geochemical affinity between the  
424 BRH tephra and the products of MMVF, plotting along the same evolutionary trend. This  
425 compositional similarity and the proximity of these tephra layers to MMVF suggest they were erupted  
426 from its vents (Figures 5 and 7). BRH major and trace element compositions plot along the  
427 evolutionary trend defined by volcanic glasses of MMVF (Figures 5 and 7), which is distinct from  
428 other volcanoes in the region. However, there is no direct match between the composition of BRH  
429 tephra and that of late Pleistocene to Holocene tephra layers exposed in the summit of Mount  
430 Melbourne, recently characterised compositionally by Del Carlo et al. (2022; MEL samples). In fact,  
431 Mount Melbourne trachytes by Del Carlo et al. (2022) are characterised by generally higher alkali  
432 and lower silica contents. In addition, Mount Melbourne summit proximal deposits lack the basaltic  
433 end-member compositions which instead are common in the BRH products except for the BRH4  
434 tephra. Thus the BRH tephra layers are likely to result from eruptions at separate vent areas, possibly  
435 from parasitic cones located on the flank of the volcano or at the periphery of the Mount Melbourne  
436 volcanic complex. On the eastern flank of Mount Melbourne, a few km NNW of Edmonson Point  
437 ropey basaltic lava and a hawaiite scoria cone are observed, known respectively as the ROL and SCC  
438 outcrops of Giordano et al. (2012). These sources are close enough and their deposits are compatible  
439 with the characteristics and the eruption styles of BRH tephra. Also, the parasitic cones NNW of the

440 summit of Mount Melbourne, that have trachytic compositions, and possibly scoria cones on the south  
441 side of Random Hills further to the north (Smellie et al., 2023) could be considered possible sources.  
442 Unfortunately, these only the eruptive centres close to Edmonson Point are dated, and not precisely.  
443 They are only constrained to the last 90 ka (Giordano et al. 2012; Smellie et al. 2023), hampering  
444 direct correlations.

445 We also compared the composition of the BRH tephra with visible tephra and cryptotephra layers  
446 identified in the marine record of the Ross Sea and in the glacial records of northern Victoria Land.  
447 Interestingly, the composition of trachytic particle population in BRH3 and BRH5, the deepest and  
448 middle tephra respectively among those studied, correlate very well with the composition of three  
449 cryptotephra recently identified in the TR17-08 piston sediment core recovered in Edisto Inlet, near  
450 Cape Hallett, more than 280 km from Melbourne volcano (Di Roberto et al. 2023; Figure 1). These  
451 cryptotephra layers, namely TR17-08-512, -518, and -524, have a trachytic composition (Figures 5  
452 and 7) and comprise colourless to light-green glass shards and pumice fragments, characterised by  
453 pristine textures among blocky, y-shaped and bubble wall morphology while preserving fragile glass  
454 tips. Within core TR17-08 tephra age was defined using radiocarbon dating of carbonate material,  
455 intercalated with tephra and was constrained between 1615 cal. years BP and 1677 cal. years BP, i.e.  
456 between the 3<sup>rd</sup> and 4<sup>th</sup> century AD (Di Roberto et al. 2023). These TR17-08 tephra layers have been  
457 interpreted as produced by a series of explosive eruptions from the Mount Melbourne volcanic  
458 complex that occurred closely spaced in time, with a maximum interval of c. 60 years between events  
459 (Di Roberto et al. 2023).

460 The geochemical correlation defined between BRH proximal tephra and distal marine tephra allows  
461 the former to be indirectly dated and consequently defines the onset (and an overall age) of this  
462 eruptive period of Mount Melbourne between the 3<sup>rd</sup> and 4<sup>th</sup> century AD. The results confirm that  
463 Mount Melbourne has been very active in historical times, with more explosive eruptive events than  
464 previously thought.

465 For the sake of completeness, it should be said that some differences exist between the BRH and  
466 TR17-08 cryptotephra. The most notable regards the lack of basaltic glass populations in TR17-08  
467 samples. The lower viscosity of the denser melts typically results in less fragmentation and lower  
468 plume heights of the basaltic phases that limit the tephra dispersal. This is consistent with the  
469 significantly larger grain size characterising the basaltic ash (and lapilli) in the studied tephra. The  
470 higher abundance of fine ash in the trachytic end-member testifies to more efficient magmatic  
471 fragmentation, and these finer particles are transported further, especially those associated with the  
472 intense phases of the eruption with high plumes. Moreover, while three cryptotephra have been  
473 identified within the TR17-08 marine core, only two tephra with similar trachytic compositions were

474 recovered at the BRH site. Another layer may be preserved deeper in the ice sequence, below the  
475 BRH5 tephra, or was eroded at the BRH site.

476 Furthermore, we explored correlations with tephra from the ice core records of Styx Glacier (SG),  
477 Talos Dome (TD) and the blue ice areas of Brimstone Peak (75.888S 158.55E; BIT Dunbar et al.  
478 2003), located at ca. 35 km, 230 km and 250 km ESE from the sampling site, respectively.  
479 Unfortunately, most of the geochemical data for SG, TD and BIT tephra layers comprise only major  
480 element glass composition for which the accuracy is not clear, and lack trace element glass data,  
481 which hamper reliable correlations with the BRH tephra layers.

482 In spite of this, we found a major similarity between the trachytic compositions of BRH4 tephra and  
483 the TD85 tephra layer in the Talos Dome record dated at c. 670 yrs BP (1280 CE; Narcisi et al. 2012;  
484 Severi et al. 2012), but it is not a viable correlation based on other tephrostratigraphic evidence. In  
485 the Talos Dome record the TD87a tephra, correlates to the 1254 CE eruption of Mount Rittmann, and  
486 is located c. two metres below the TD85 (Severi et al. 2012). Given that the 1254 CE tephra is  
487 ubiquitous in the marine and glacial records of the Ross Sea and northern Victoria Land, a significant  
488 and widespread tephra marker (Di Roberto et al. 2019 and references therein), and it is not between  
489 BRH4 and BRH5 in the proximal exposure we conclude that BRH4 does not correlate to TD85.

490 A tephrostratigraphy similar to that of Talos Dome has been developed for the Styx glacier ice core  
491 (which is the ice record closer to the studied BRH site), where the 1254 CE tephra was detected at a  
492 depth of 99.18 m and is only overlaid by another tephra at 97.01 m (Han et al. 2015), instead of five  
493 ash layers.

494 Vice versa, our data confirm that TD85 likely derives from Mount Melbourne volcanic activity, as  
495 previously suggested by Narcisi et al. (2012), based on the major element data. If this correlation  
496 would be verified using trace element glass compositions, it would affirm that Mount Melbourne was  
497 active in even more recent times, less than 700 years ago. This further shows that incomplete  
498 geochemical databases strongly limit correlation efficacy, and high-quality geochemical data are  
499 necessary to make reliable correlations.

500 A general geochemical affinity also exists between BRH1, BRH2, and BRH5 tephra and the  
501 composition of BIT volcanic ash (Dunbar 2003). In detail, there is a strong similarity in major element  
502 compositions between the BRH1, BRH2, and BRH5 basalt to basanite glass population and the  
503 BIT121 and BIT122 ash layers (Fig. 5). Trace elements compositions of BIT are not entirely  
504 determined, and the same similarity can be only documented in the Th vs Hf plot (Fig. 7d). BIT121  
505 and BIT122 layers are respectively a thick dark brown unit made of clear, aphyric, and dense blocky  
506 shards (BIT121) and a grey diffuse layer with clear to olive green glass, blocky shards with spherical  
507 vesicles, plus droplets and glass hairs. In particular, the latter has strikingly similar textural

508 characteristics to the BRH tephra. Unfortunately, BIT volcanic ash layers lack chronological and  
509 appropriate trace elements information, and thus cannot be definitively correlated with BRH.

510

#### 511 *4.2 Eruption dynamics*

512 Componentry, textures, and geochemical fingerprints of the studied tephra indicate that these layers  
513 have been emplaced as primary fallout deposits. As mentioned above the external morphology of  
514 particles that preserves pristine features like fragile glass tips, Pele's hair, or spiny glass edges (Figures  
515 3 and 4) and glass coatings around magmatic crystals indicate minor or no aeolian remobilization, re-  
516 sedimentation, or other transport after deposition from the volcanic plume.

517 The volcanic glass composition of each sample, which is strongly bimodal with other analyses along  
518 geochemical trends, always lies on the same evolutionary compositional lineage indicating the same  
519 volcanic source (see Del Carlo et al. 2018). The proximity of these decimeter-thick units to the  
520 MMVF, and their shared geochemical affinity is consistent being from Mt. Melbourne or other vents  
521 around the summit. The absence of large amounts of detrital material, including glass particles from  
522 other volcanic sources is evident and indicates negligible reworking, re-sedimentation, and  
523 redistribution of pyroclastic products.

524 Glass particles forming the studied deposits comprise a variety of fragments differing in external  
525 shape, vesicularity, mineral content, and composition. Internal and external textural inhomogeneity  
526 is widely documented in the products of explosive eruptions from many volcanoes and has been  
527 ascribed to changes in the ascent and/or flow conditions during the eruption and to diverse  
528 mechanisms of particle fragmentation (i.e. hydromagmatic vs magmatic), transport and the eruptive  
529 environment (see e.g., D'Oriano et al. 2022 and references therein).

530 The almost ubiquitous presence of fluidal fragments including Pele's hair and tears (i.e. fibres and  
531 droplets of volcanic glass; Figures 3 and 4) indicate specific eruptive dynamics and magma properties  
532 typical of magmatic eruptions. Fluidal fragments and Pele's hairs and tears formed by the stretching,  
533 deformation, and final magma breakup of very hot, low-viscosity magma due to interfacial shear  
534 between gas and melt (see Lin and Reitz 1998; Eggers and Villermaux 2008). Pele's hairs and tears  
535 form during subaerial Hawaiian-style eruptions fed by low-viscosity basaltic melts (Heiken and  
536 Wohletz 1985) and are also common, but minor, in basaltic eruptions occurring in sub-aqueous  
537 environments (Clague et al. 2000, 2003). Similarly, the presence of abundant moderately to highly  
538 vesicular basaltic particles with cusped to spongy external surfaces is indicative of pure magmatic  
539 fragmentation of gas-rich melts dominated by exsolution and expansion of magmatic gas for example  
540 in a Strombolian column.

541 More equant and blocky particles have irregular contours, are bounded by sharp planar edges and are  
542 made of dense to poorly vesicular glass, bearing features like stepped surfaces and quenching cracks,  
543 as well as hackle lines and surface pitting (Figures 4i-l), which are distinctive of phreatomagmatic  
544 fragmentation (Fisher and Schmincke 1984; Heiken and Wohletz 1985; Morrissey et al. 2000; Durig  
545 et al. 2012; Zimanowski et al. 2015; Ross et al. 2021). Stepped features are a consequence of the  
546 extreme and intensive brittle fracturing of the melt (Zimanowski et al. 2015). The water, in direct  
547 contact with the hot melt, expands and exerts a massive hydraulic pressure onto the melt itself, which  
548 behaves in a brittle way, so that cracks are occurring, driven by the applied stress; still liquid water is  
549 pushed into the propagating crack, thus increasing the interface area between magma and water and  
550 therefore increasing the heat flux from magma to water, generating an accelerating thermohydraulic  
551 feedback loop (Durig and Zimanowski 2012; Durig et al. 2012). Hackle lines indicate the direction  
552 of propagation of a crack and, since these can form during slow or fast cracking, are not strictly  
553 diagnostic of melt-water interaction, although some fragmentation experiments with water produce  
554 increased proportions of particles with hackle lines relative to others without water (Ross et al. 2022).  
555 Quenching cracks form immediately after fragmentation due to the sudden quenching and consequent  
556 contraction of still-hot particles due to the fast contact with liquid water (Zimanowski et al. 2015).  
557 Pitted surfaces indicate incipient alteration resulting from the interaction of glass with hydrothermal  
558 fluids (or excess water) in the eruptive column (Zimanowski et al. 2015; Ross et al. 2022).

559 The simultaneous presence of particle morphologies with features indicative of magmatic and  
560 hydromagmatic fragmentation in BRH tephra layers is evidence that various degrees of magma-water  
561 interaction occurred during the forming eruptions. For example, texturally mixed deposits could  
562 derive from the transformation of an initially subglacial, hydromagmatic eruption fuelled by the  
563 interaction between magma and meltwater, into a relatively dry magmatic subaerial Hawaiian to  
564 Strombolian-style eruption, once the water source was exhausted, drained or the magma no longer  
565 came into contact with the meltwater (vent completely subaerial). As mentioned above, the major and  
566 trace element glass compositions of the heterogeneous BRH1 to 5 tephra deposits are largely  
567 overlapping, and clearly reside on the same evolutionary trends indicating they all likely derive from  
568 the same magmatic system. The overall chemical variability (ranging from basalts through to  
569 trachytes) and in particular the observed clustering of the erupted volcanic glass compositions along  
570 the overall evolutionary trend might indicate that the successive eruptions were fed by a complex and  
571 vertically extensive magma storage region beneath the source volcano (Cashman et al. 2017;  
572 Giordano and Caricchi, 2022). This is quite common as reported for several eruptions (see Shane et  
573 al. 2002, 2007, 2008).

574 Interestingly, apart from BRH4, all the remaining BRH tephra deposits comprise a basaltic glass  
575 component, and the interaction of the mafic melt with more evolved trachy-andesitic to trachytic  
576 magma pockets, or mush, is the likely trigger of these eruptions. In this regard, it should be  
577 highlighted that at least during some of the eruptive phases emplacing BRH tephra a trachytic magma  
578 was fragmented efficiently enough to disperse the ash several hundred kilometres away. This is  
579 possible only during high-intensity eruptions able to produce eruptive columns of significant heights,  
580 as hypothesised by Di Roberto et al. (2023).

581

## 582 **5. Conclusions**

583 BRH1 to 5 tephra are primary fallout layers derived from five explosive eruptions that occurred in a  
584 short time from within the Mount Melbourne Volcanic Field. The nature and texture of particles  
585 forming the tephra layers indicate that the eruptions were mostly Hawaiian to Strombolian in style  
586 and characterized by magmatic and possibly hydromagmatic fragmentation occurring over the time  
587 of the eruption. The distal dispersal of trachytic ashes to some hundreds of km from the source (c.  
588 280 km) also demonstrates that the BRH eruptions were at some time characterised by a strong  
589 explosivity and very efficient magma fragmentation, and possibly produced several km-high eruptive  
590 columns.

591 The magma compositions feeding the eruptions range from basalts to trachytes and the clustering of  
592 the erupted products compositions indicate that the eruptions were fed by a complex and vertically  
593 extensive magma system region beneath the source volcano with the mafic melt remobilizing more  
594 evolved trachy-andesitic to trachytic magma pockets.

595 Although the geochemical data confirm that the volcanic source of BRH1 to 5 tephra is the Mount  
596 Melbourne volcano, there is no direct match between the composition of tephra studied here and  
597 Pleistocene to Holocene tephra layers exposed in the summit part of Mount Melbourne characterised  
598 by Del Carlo et al. (2022; MEL samples). This potentially indicates that BRH tephra originated from  
599 vents located away from the summit area.

600 The geochemical correlations assessed between the BRH tephra deposits and three marine  
601 cryptotephra intercalated in sediments of the Edisto Inlet (TR17-08-512, -518, and -524), which were  
602 dated by the radiocarbon method between 1615 cal. yrs BP and 1677 cal. yrs BP., allowed to  
603 indirectly constrain the ages of BRH eruptions between the 3<sup>rd</sup> and 4<sup>th</sup> century CE. This finding  
604 improves our knowledge of the eruptive history of Mount Melbourne volcano, which has produced  
605 at least five eruptions during historical time, increasing the awareness of potential hazards to the  
606 several permanent scientific bases close to Mount Melbourne.



607 Moreover, the attribution of a numerical age to the BRH tephra elevates them to new regional  
608 isochron markers that will possibly enhance the correlation and synchronisation of climatic records  
609 of the northern Victoria Land and Ross Sea areas.

610 This study demonstrates once again the great robustness of the tephrochronological method in terms  
611 of correlation and dating of glacial, terrestrial and marine records, if carried out with a modern  
612 approach and up-to-date techniques. The need for high-quality textural, mineralogical and  
613 compositional data (major and trace element glass compositions) on tephra is even more evident for  
614 Antarctica, where outcrops are scarce. Only with an exhaustive fingerprinting of tephra layers, it is  
615 possible to establish effective correlations between different records enhancing synchronisation and  
616 correlations for paleoenvironmental and paleoclimatic reconstructions.

617

### 618 **Acknowledgements**

619 This work was funded by the Projects: ICE-VOLC (multiparametric Experiment at Antarctica  
620 VOLCanoes: data from volcano and cryosphere-ocean-atmosphere dynamics, [www.icevolc-](http://www.icevolc-project.com/)  
621 [project.com/](http://project.com/); PNRA 14\_00011), TRACERS (Tephrochronology and marker events for the  
622 Correlation of natural archives in the Ross Sea, Antarctica; PNRA2016 - Linea A3/00055) and  
623 CHIMERA (Cryptotephra In Marine Sequences of the Ross Sea, Antarctica: implications and  
624 potential applications; PNRA18\_00158-A). We acknowledge PNRA, the Italian Programma  
625 Nazionale di Ricerche in Antartide, for funding the projects and ENEA for providing field logistics  
626 at Mario Zucchelli Station. We are grateful to the pilots J. Henery and B. McElhinney for the  
627 helicopter surveys and the Italian alpine guides M. Bussani and D. De Podestà for sampling the ice  
628 cliff and their assistance in the fieldwork. Dr C. Manning is also acknowledged for her assistance  
629 with the LA-ICP-MS analysis. We also thank the Editor J.L. Smellie, G. Giordano and an anonymous  
630 reviewer for their revisions that greatly improved the paper. This paper is sponsored by the SCAR  
631 Expert Group, *AntVolc* and in memory of Antonio De Sio (Tony), an Antarctic friend of ours.

632

### 633 **Credit author statement**

634 P.D.C., A.C., G.G. and G.L. carried out the fieldwork and sampling on the flanks of Mt. Melbourne.  
635 P.D.C. and A.D.R. conceived the research. P.D.C., A.D.R., G.R. and B.S. carried out the textural  
636 analysis of the volcanic glass, the petrographic analysis and interpreted geochemical and petrological  
637 data. P.G.A. and V.C.S. carried out the major- and trace element geochemical analyses, respectively.  
638 All authors contributed to data interpretation, the writing of the manuscript and the preparation of the  
639 figures.

640

641 **References**

642 Adamson RG, Cavaney RJ (1967) Volcanic Debris-Layers near Mount Melbourne, Northern Victoria  
643 Land, Antarctica. *New Zeal J Geol Geophys* 10:418–421.  
644 <https://doi.org/10.1080/00288306.1967.10426745>

645  
646 Armienti P, Civetta L, Innocenti F, Manetti P, Tripodo S, Villari L, Vita G (1991) New petrological  
647 and geochemical data on Mt. Melbourne Volcanic Field, Northern Victoria Land, Antarctica. (II  
648 Italian Antarctic Expedition). *Mem Soc Geol It* 46:397-424.

649  
650 Cashman KV, Sparks RSJ, Blundy JD (2017) Vertically extensive and unstable magmatic systems:  
651 A unified view of igneous processes *Science* 355 eaag3055-11.  
652 <https://doi.org/10.1126/science.aag3055>

653  
654 Clague DA, Moore JG, Reynolds JR (2000) Formation of submarine flat-topped volcanic cones in  
655 Hawai'i. *Bull Volcanol* 62:214–233. <https://doi.org/10.1007/s004450000088>

656  
657 Clague DA, Batiza R, Head JW, Davis AS (2003) Pyroclastic and Hydroclastic Deposits on Loihi  
658 Seamount, Hawaii. In: *Explosive Subaqueous Volcanism*. AGU Geophys Monogr 140:73–95  
659 <https://doi.org/10.1029/140GM05>

660  
661 Curzio P, Folco L, Ada Laurenzi M, et al (2008) A tephra chronostratigraphic framework for the  
662 Frontier Mountain blue-ice field (northern Victoria Land, Antarctica). *Quat Sci Rev* 27:602–620.  
663 <https://doi.org/https://doi.org/10.1016/j.quascirev.2007.11.017>

664  
665 Del Carlo P, Di Roberto A, Di Vincenzo G, Bertagnini A, Landi P, Pompilio M, Colizza E, Giordano  
666 G (2015) Late Pleistocene-Holocene volcanic activity in northern Victoria Land recorded in Ross Sea  
667 (Antarctica) marine sediments. *Bull Volcanol* 77:36. <https://doi.org/10.1007/s00445-015-0924-0>

668  
669 Del Carlo P, Di Roberto A, D'Orazio M, Petrelli M, Angioletti A, Zanchetta G, Maggi V, Daga R,  
670 Nazzari M, Rocchi S (2018). Late Glacial-Holocene tephra from southern Patagonia and Tierra del  
671 Fuego (Argentina, Chile): A complete textural and geochemical fingerprinting for distal correlations  
672 in the Southern Hemisphere. *Quaternary Science Reviews*, 195, 153-170.  
673 <https://doi.org/10.1016/j.quascirev.2018.07.028>

674

675 Del Carlo P, Di Roberto A, Di Vincenzo G, Re G, Albert PG, Nazzari M, Smith VC, Cannata A  
676 (2022) Tephrostratigraphy of proximal pyroclastic sequences at Mount Melbourne (northern Victoria  
677 Land, Antarctica): Insights into the volcanic activity since the last glacial period. *J Volcanol*  
678 *Geotherm Res* 422:107457. <https://doi.org/https://doi.org/10.1016/j.jvolgeores.2021.107457>  
679

680 Di Roberto A, Colizza E, Del Carlo P, Petrelli M, Finocchiaro F, Kuhn G (2019) First marine  
681 cryptotephra in Antarctica found in sediments of the western Ross Sea correlates with englacial  
682 tephras and climate records. *Sci Rep* 9:10628. <https://doi.org/10.1038/s41598-019-47188-3>  
683

684 Di Roberto A, Albert PG, Colizza E, Del Carlo P, Di Vincenzo G, Gallerani A, Giglio F, Kuhn G,  
685 Macrì P, Manning CJ, Melis R, Miseroocchi S, Scateni B, Smith VC, Torricella F, Winkler A (2020)  
686 Evidence for a large-magnitude Holocene eruption of Mount Rittmann (Antarctica): A volcanological  
687 reconstruction using the marine tephra record. *Quat Sci Rev* 250:106629.  
688 <https://doi.org/https://doi.org/10.1016/j.quascirev.2020.106629>  
689

690 Di Roberto A, Scateni B, Di Vincenzo G, Petrelli M, Fisauli G, Barker SJ, Del Carlo P, Colleoni F,  
691 Kulhanek DK, McKay R, De Santis L (2021a) Tephrochronology and Provenance of an Early  
692 Pleistocene (Calabrian) Tephra From IODP Expedition 374 Site U1524, Ross Sea (Antarctica).  
693 *Geochemistry, Geophys Geosystems* 22:e2021GC009739.  
694 <https://doi.org/https://doi.org/10.1029/2021GC009739>  
695

696 Di Roberto A, Del Carlo P, Pompilio M (2021b) Chapter 6.1 Marine record of Antarctic volcanism  
697 from drill cores. *Geol Soc London, Mem* 55:631 LP – 647. <https://doi.org/10.1144/M55-2018-49>  
698

699 Di Roberto A, Re G, Scateni B, Petrelli M, Tesi T, Capotondi L, Morigi C, Galli G, Colizza E, Melis  
700 R, Torricella F, Giordano P, Giglio F, Gallerani A, Gariboldi K (2023). Cryptotephras in the marine  
701 sediment record of the Edisto Inlet, Ross Sea: Implications for the volcanology and tephrochronology  
702 of northern Victoria Land, Antarctica. *Quat Sci Adv* 100079.  
703 <https://doi.org/https://doi.org/10.1016/j.qsa.2023.100079>  
704

705 D’Oriano C, Del Carlo P, Andronico D, Cioni R, Gabellini P, Cristaldi A, Pompilio M (2022) Syn-  
706 Eruptive Processes During the January–February 2019 Ash-Rich Emissions Cycle at Mt. Etna (Italy):  
707 Implications for Petrological Monitoring of Volcanic Ash. *Front Earth Sci* 10:824872.  
708 <https://doi.org/10.3389/feart.2022.824872>

709

710 Dunbar N (2003) Blue Ice Tephra II - Brimstone Peak. U.S. Antarctic Program (USAP) Data Center.

711 <https://doi.org/10.7265/N5MG7MDK>

712

713 Dunbar NW, Zielinski GA, Voisins DT (2003) Tephra layers in the Siple Dome and Taylor Dome  
714 ice cores, Antarctica: Sources and correlations. *J Geophys Res Solid Earth* 108:2374.

715 <https://doi.org/10.1029/2002JB002056>

716

717 Dürig T, Zimanowski B (2012) “Breaking news” on the formation of volcanic ash: Fracture dynamics  
718 in silicate glass. *Earth Planet Sci Lett* 335–336:1–8.

719 <https://doi.org/https://doi.org/10.1016/j.epsl.2012.05.001>

720

721 Dürig T, Mele D, Dellino P, Zimanowski B (2012) Comparative analyses of glass fragments from  
722 brittle fracture experiments and volcanic ash particles. *Bull Volcanol* 74:691–704.

723 <https://doi.org/10.1007/s00445-011-0562-0>

724

725 Eggers J, Villiermaux E (2008) Physics of liquid jets. *Reports Prog Phys* 71:36601.

726 <https://doi.org/10.1088/0034-4885/71/3/036601>

727

728 Fisher RV, Schmincke J-U (1984) *Pyroclastic Rocks*. Springer-Verlag, Berlin.

729 <http://dx.doi.org/10.1007/978-3-642-74864-6>

730

731 Gambino S, Armienti P, Cannata A, Del Carlo P, Giudice G, Giuffrida G, Liuzzo M, Pompilio M  
732 (2021) Chapter 7.3 Mount Melbourne and Mount Rittmann. *Geol Soc London, Mem* 55:M55-2018–

733 43. <https://doi.org/10.1144/M55-2018-43>

734

735 Geyer A (2021) Chapter 1.4 Antarctic volcanism: active volcanism overview. *Geol Soc London,*  
736 *Mem* 55:M55-2020–12. <https://doi.org/10.1144/M55-2020-12>

737

738 Giordano G and Caricchi L (2022) Determining the state of activity of transcrustal magmatic systems  
739 and their volcanoes." *Annual Review of Earth and Planetary Sciences* 50 (2022): 231-259.

740 <https://doi.org/10.1146/annurev-earth-032320-084733>

741

742 Giordano G, Lucci F, Phillips D, Cozzupoli D, Runci V (2012) Stratigraphy, geochronology and  
743 evolution of the Mt. Melbourne volcanic field (North Victoria Land, Antarctica). *Bull Volcanol*  
744 74:1985–2005. <https://doi.org/10.1007/s00445-012-0643-8>  
745

746 Han Y, Jun SJ, Miyahara M, Lee H, Ahn J, Chung JW, Hur SD, Hong SB (2015) Shallow ice-core  
747 drilling on Styx glacier, northern Victoria Land, Antarctica in the 2014-2015 summer TT. *J Geol Soc*  
748 Korea 51(3):343–355 <https://doi.org/10.14770/jgsk.2015.51.3.343>  
749

750 Harpel CJ, Kyle PR, Dunbar NW (2008) Englacial tephrostratigraphy of Erebus volcano, Antarctica.  
751 *J Volcanol Geotherm Res* 177:549–568.  
752 <https://doi.org/https://doi.org/10.1016/j.jvolgeores.2008.06.001>  
753

754 Heiken G, Wohletz K (1985) *Volcanic Ash*. Berkeley, University of California Press  
755

756 Iverson NA, Kyle PR, Dunbar NW, McIntosh WC, Pearce NJG (2014) Eruptive history and magmatic  
757 stability of Erebus volcano, Antarctica: Insights from englacial tephra. *Geochemistry, Geophys*  
758 *Geosystems* 15:4180–4202. <https://doi.org/https://doi.org/10.1002/2014GC005435>  
759

760 Iverson NA, Kalteyer D, Dunbar NW, Kurbatov A, Yates M (2017) Advancements and best practices  
761 for analysis and correlation of tephra and cryptotephra in ice. *Quat Geochronol* 40:45–55.  
762 <https://doi.org/https://doi.org/10.1016/j.quageo.2016.09.008>  
763

764 Jochum KP, Pfänder J, Woodhead JD, Willbold M, Stoll B, Herwig K, Amini M, Abouchami W,  
765 Hofmann AW (2005) MPI-DING glasses: New geological reference materials for in situ Pb isotope  
766 analysis. *Geochemistry, Geophys Geosystems* 6.  
767 <https://doi.org/https://doi.org/10.1029/2005GC000995>  
768

769 Jochum KP, Stoll B, Herwig K, Willbold M, Hofmann AW, Amini M, Aarburg S, Abouchami W,  
770 Hellebrand E, Mocek B, Raczek I, Stracke A, Alard O, Bouman C, Becker S, Dücking M, Brätz H,  
771 Klemd R, de Bruin D, Canil D, Cornell D, de Hoog C, Dalpé C, Danyushevsky L, Eisenhauer A, Gao  
772 Y, Snow JE, Groschopf N, Günther D, Latkoczy C, Guillong M, Hauri E, Höfer HE, Lahaye Y, Horz  
773 K, Jacob DE, Kasemann SA, Kent AJR, Ludwig T, Zack T, Mason PRD, Meixner A, Rosner M,  
774 Misawa K, Nash BP, Pfänder J, Premo WR, Sun WD, Tiepolo M, Vannucci R, Vennemann T, Wayne  
775 D, Woodhead JD (2006) MPI-DING reference glasses for in situ microanalysis: New reference values

776 for element concentrations and isotope ratios. *Geochemistry, Geophys Geosystems* 7(2).  
777 <https://doi.org/10.1029/2005GC001060>  
778

779 Hillenbrand C, Moreton SG, Caburlotto A, Pudsey CJ, Lucchi RG, Smellie JL, Benetti S, Grobe H,  
780 Hunt JB, Larter RD (2008) Volcanic time-markers for Marine Isotopic Stages 6 and 5 in Southern  
781 Ocean sediments and Antarctic ice cores: implications for tephra correlations between palaeoclimatic  
782 records. *Quaternary Science Reviews*, 27, 518-540. <https://doi.org/10.1016/j.quascirev.2007.11.009>  
783

784 Kim D, Prior DJ, Han Y, Qi C, Han H, Ju HT (2020) Microstructures and Fabric Transitions of  
785 Natural Ice from the Styx Glacier, Northern Victoria Land, Antarctica. *Minerals* 10:892.  
786 <https://doi.org/10.3390/min10100892>  
787

788 Kurbatov AV, Zielinski GA, Dunbar NW, Mayewski PA, Meyerson EA, Sneed SB, Taylor KC  
789 (2006) A 12,000 year record of explosive volcanism in the Siple Dome Ice Core, West Antarctica. *J*  
790 *Geophys Res Atmos* 111:D12307. <https://doi.org/https://doi.org/10.1029/2005JD006072>  
791

792 LeBas MJL, Maitre RWL, Streckeisen A, Zanettin B, IUGS Subcommittee on the Systematics of  
793 Igneous Rocks (1986) A Chemical Classification of Volcanic Rocks Based on the Total Alkali-Silica  
794 Diagram. *J Petrol* 27:745–750. <https://doi.org/10.1093/petrology/27.3.745>  
795

796 Lee MJ, Kyle PR, Iverson NA, Lee JI, Han Y (2019) Rittmann volcano, Antarctica as the source of  
797 a widespread 1252 ± 2 CE tephra layer in Antarctica ice. *Earth Planet Sci Lett* 521:169–176.  
798 <https://doi.org/https://doi.org/10.1016/j.epsl.2019.06.002>  
799

800 Lin SP, Reitz RD (1998) Drop and spray formation from a liquid jet. *Ann Rev Fluid Mech* 30:85–  
801 105. <https://doi.org/10.1146/annurev.fluid.30.1.85>  
802

803 Lyon GL (1986) Stable isotope stratigraphy of ice cores and the age of the last eruption at Mount  
804 Melbourne, Antarctica. *New Zeal J Geol Geophys* 29:135–138.  
805 <https://doi.org/10.1080/00288306.1986.10427528>  
806

807 Lowe DJ (2011) Tephrochronology and its application: A review. *Quaternary Geochronology*, 6, 107-  
808 153, <https://doi.org/10.1016/j.quageo.2010.08.003>  
809

810 McDonough WF, Sun S-s. (1995) The composition of the Earth. *Chem Geol* 120:223–253.  
811 [https://doi.org/10.1016/0009-2541\(94\)00140-4](https://doi.org/10.1016/0009-2541(94)00140-4)  
812

813 Morrissey M, Zimanowski B, Wohletz K, Buettner R (2000) Phreatomagmatic fragmentation. In:  
814 Sigurdsson H, Houghton B, McNutt SR, Rymer H, Stix J (eds) *Encyclopedia of volcanoes*. Academic,  
815 London, pp 431–445  
816

817 Narcisi B, Petit JR, Delmonte B, Basile-Doelsch I, Maggi V (2005) Characteristics and sources of  
818 tephra layers in the EPICA-Dome C ice record (East Antarctica): Implications for past atmospheric  
819 circulation and ice core stratigraphic correlations. *Earth Planet Sci Lett* 239:253–265.  
820 <https://doi.org/10.1016/j.epsl.2005.09.005>  
821

822 Narcisi B, Petit JR, Delmonte B, Scarchilli C, Stenni B (2012) A 16,000-yr tephra framework for the  
823 Antarctic ice sheet: a contribution from the new Talos Dome core. *Quat Sci Rev* 49:52–63.  
824 <https://doi.org/10.1016/j.quascirev.2012.06.011>  
825

826 Narcisi B, Petit JR (2021) Chapter 6.2 Englacial tephtras of East Antarctica. *Geol Soc London, Mem*  
827 55:649 LP-664. <https://doi.org/10.1144/M55-2018-86>  
828

829 Nardin R, Severi M, Amore A, Becagli S, Burgay F, Caiazzo L, Ciardini V, Dreossi G, Frezzotti M,  
830 Hong S-B, Khan I, Narcisi BM, Proposito M, Scarchilli C, Selmo E, Spolaor A, Stenni B, Traversi R  
831 (2021) Dating of the GV7 East Antarctic ice core by high-resolution chemical records and focus on  
832 the accumulation rate variability in the last millennium. *Clim Past* 17:2073–2089.  
833 <https://doi.org/10.5194/cp-17-2073-2021>  
834

835 Panter, KS (2021). Antarctic volcanism: petrology and tectonomagmatic overview. *Geol Soc Lond*  
836 *Mem* 55:43-53. <https://doi.org/10.1144/M55-2020-10>  
837

838 Peccerillo A, Taylor SR (1976) Geochemistry of eocene calc-alkaline volcanic rocks from the  
839 Kastamonu area, Northern Turkey. *Contrib to Mineral Petrol* 58:63–81.  
840 <https://doi.org/10.1007/BF00384745>  
841

842 Rocchi S, Smellie JL (2021) Chapter 5.1b Northern Victoria Land: petrology. *Geol Soc London,*  
843 *Mem* 55:383 LP – 413. <https://doi.org/10.1144/M55-2019-19>

844

845 Ross P-S, Dürig T, Comida PP, Lefebvre N, White JDL, Andronico D, Thivet S, Eychenne J, Gurioli  
846 L (2021) Standardized analysis of juvenile pyroclasts in comparative studies of primary magma  
847 fragmentation; 1. Overview and workflow. Bull Volcanol 84:13. [https://doi.org/10.1007/s00445-021-](https://doi.org/10.1007/s00445-021-01516-6)  
848 [01516-6](https://doi.org/10.1007/s00445-021-01516-6)

849

850 Severi M, Udisti R, Becagli S, Stenni B, Traversi R (2012) Volcanic synchronisation of the EPICA-  
851 DC and TALDICE ice cores for the last 42 kyr BP. Clim Past 8:509–517. [https://doi.org/10.5194/cp-](https://doi.org/10.5194/cp-8-509-2012)  
852 [8-509-2012](https://doi.org/10.5194/cp-8-509-2012)

853

854 Shane P and Hoverd J (2002) Distal record of multi-sourced tephra in Onepoto Basin, Auckland, New  
855 Zealand: implications for volcanic chronology, frequency and hazards. Bull Volcanol 64: 441–54.  
856 <https://doi.org/10.1007/s00445-002-0217-2>

857

858 Shane P, Martin SB, Smith VC, Beggs KF, Darragh MB, Cole JW and Nairn IA (2007) Multiple  
859 rhyolite magmas and basalt injection in the 17.7 ka Rerewhakaaitu eruption episode from Tarawera  
860 volcanic complex. New Zealand J Volcanol Geotherm Res 164: 1–26.  
861 <https://doi.org/10.1016/j.jvolgeores.2007.04.003>

862

863 Shane P, Nairn I A, Smith V C, Darragh M, Beggs K and Cole J W (2008) Silicic recharge of multiple  
864 rhyolite magmas by basaltic intrusion during the 22.6 ka Okareka Eruption Episode, New Zealand.  
865 LITHOS 103: 527–49. <https://doi.org/10.1016/j.lithos.2007.11.002>

866

867 Smellie JL (1999) The upper Cenozoic tephra record in the south polar region: a review. Glob Planet  
868 Change 21:51–70. [https://doi.org/10.1016/S0921-8181\(99\)00007-7](https://doi.org/10.1016/S0921-8181(99)00007-7)

869

870 Smellie JL, Rocchi S (2021) Northern Victoria Land: volcanology. Geological Society, London,  
871 Memoirs, 55. <https://doi.org/10.1144/M55-2018-60>

872

873 Smellie, JL, Rocchi S, Di Vincenzo G (2023) Controlling influence of water and ice on eruptive style  
874 and edifice construction in the Mount Melbourne Volcanic Field (northern Victoria Land, Antarctica).  
875 Frontiers in Earth Science - Volcanology, 10:1061515. <https://doi.org/10.3389/feart.2022.1061515>

876



877 Tomlinson EL, Thordarson T, Müller W, Thirlwall M, Menzies MA (2010) Microanalysis of tephra  
878 by LA-ICP-MS - Strategies, advantages and limitations assessed using the Thorsmörk ignimbrite  
879 (Southern Iceland). *Chem Geol* 279:73–89. <https://doi.org/10.1016/j.chemgeo.2010.09.013>

880

881 Wolff EW, Barbante C, Becagli S, Bigler M, Boutron CF, Castellano E, de Angelis M, Federer U,  
882 Fischer H, Fundel F, Hansson M, Hutterli M, Jonsell U, Karlin T, Kaufmann P, Lambert F, Littot  
883 GC, Mulvaney R, Röthlisberger R, Ruth U, Severi M, Siggaard-Andersen ML, Sime LC, Steffensen  
884 JP, Stocker TF, Traversi R, Twarloh B, Udisti R, Wagenbach D, Wegner A (2010) Changes in  
885 environment over the last 800,000 years from chemical analysis of the EPICA Dome C ice core. *Quat*  
886 *Sci Rev* 29(1–2):285–295. <https://doi.org/https://doi.org/10.1016/j.quascirev.2009.06.013>

887

888 Zimanowski B, Büttner R, Delino P, White JDL, Wohletz K (2015) Magma-water interaction and  
889 phreatomagmatic fragmentation. In: Sigurdsson H, Houghton B, McNutt SR, Rymer H, Stix J (eds)  
890 *Encyclopedia of Volcanoes*, 2nd edn. Academic Press, London, pp 473–484

891

892

### 893 **Figure captions**

894

895 **Figure 1.** a) Map of the volcanoes in northern Victoria Land. The location of the studied outcrop is  
896 labelled with a red star whereas the location of the marine sediment core TR17-08 in Edisto Inlet (Di  
897 Roberto et al. 2023) and of the deep ice cores at Talos Dome and Styx glacier are annotated with a  
898 green star and blue hexagons, respectively. Green dots indicate the location of the permanent  
899 scientific bases. The red box outlines the area of the topographic map in (b) that illustrate Mount  
900 Melbourne and locations of the BRH sections. c) Picture of the studied outcrop where the BRH tephra  
901 layers are exposed, Mount Melbourne in the background.

902

903 **Figure 2.** Picture of the glacier cliff where BRH tephra layers are exposed, taken during the sampling  
904 performed by the Italian alpine guides. On the picture are annotated the five englacial tephra and the  
905 ice thickness between them.

906

907 **Figure 3.** Optical stereo-microscope images of a BRH4 ash. Images in the small boxes represent the  
908 different types of components. A) Vesicular; B) Blocky; C) Pele's tear; D) Spiny fluidal; E)  
909 Lithicclast; F) Pumice; G) Vesicular fragment with sharp-planar breakage surface.

910

911 **Figure 4.** Back-scattered electron (BSE) images of the studied tephra; A) BRH1; B) BRH2; C)  
912 BRH3; D) BRH4; E) BRH5. Letters annotated within these five pictures represent the different types  
913 of components: B - Blocky; F - Fluidal; L - Lithic clast; V - Vesicular pumice fragment. Secondary  
914 electron images (F-N) of 3D silhouettes of selected clasts illustrating the morphology of magmatic  
915 (F-H) and phreatomagmatic (I-N) juvenile clasts. Yellow arrows indicate stepped features and hackle  
916 marks, blue arrows point at branching quenching cracks, and the red arrow highlights pitted surfaces.  
917

918 **Figure 5.** Bivariate major element plots depicting the significant volcanic glass heterogeneity of the  
919 BRH1 to 5 tephra deposits which range from basalts through to trachytes. (A) Total alkalis vs. silica  
920 classification diagram (TAS) following LeBas et al. (1986); (B)  $K_2O$  vs.  $SiO_2$  following Peccerillo  
921 and Taylor (1976). The trachytic glasses of the BRH 1 to 5 tephra layers plot along the same evolution  
922 trend as those previously analysed from Mount Melbourne (Del Carlo et al., 2022), and are offset  
923 from glasses erupted at nearby volcanic centres, such as Mount Rittmann (Di Roberto et al., 2019),  
924 The Pleiades (Lee et al., 2019) and Mount Erebus (Harpel et al., 2008). Black dashed line encircle  
925 The gray compositional field represents the TR17-08 tephra from Edisto Inlet and the black symbols  
926 indicate tephra from Brimstone Peak (BIT121, × BIT122; Dunbar 2003).  
927

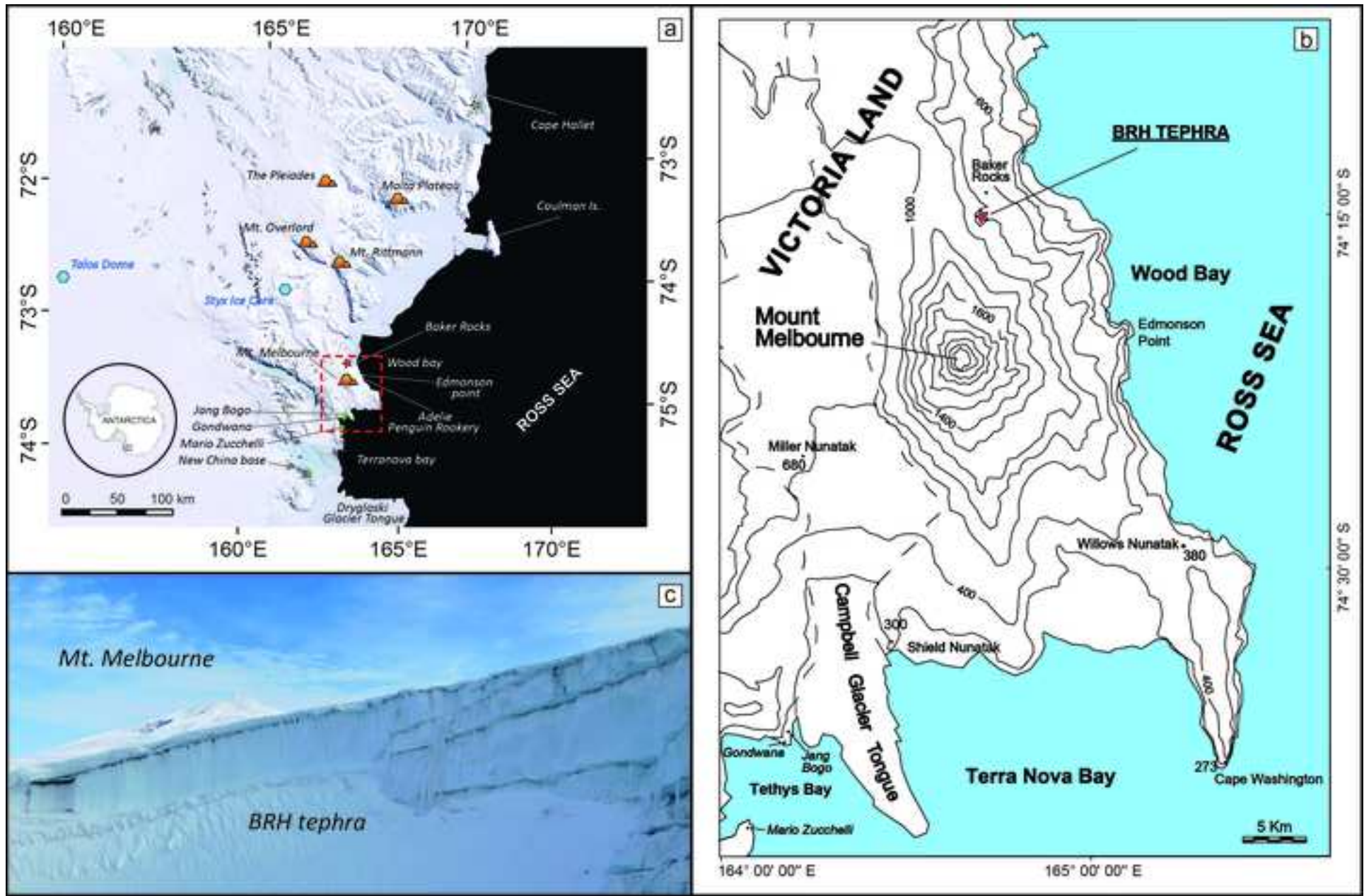
928 **Figure 6.** Primitive mantle normalised (McDonough and Sun 1995) trace element concentrations of  
929 volcanic glass (component averages) for the BRH1 to 5 tephra layers. The data presented clearly  
930 illustrate a chemical link between the trachytic end-member glasses of the BRH tephra layers and  
931 those found at the summit of Mount Melbourne (Del Carlo et al., 2022). Bas = basalt; Tra-Bas =  
932 trachy-basalt; Bas Tra-And = basaltic trachy-andesite; Tra-And = trachy-andesite; Tra = trachyte.  
933

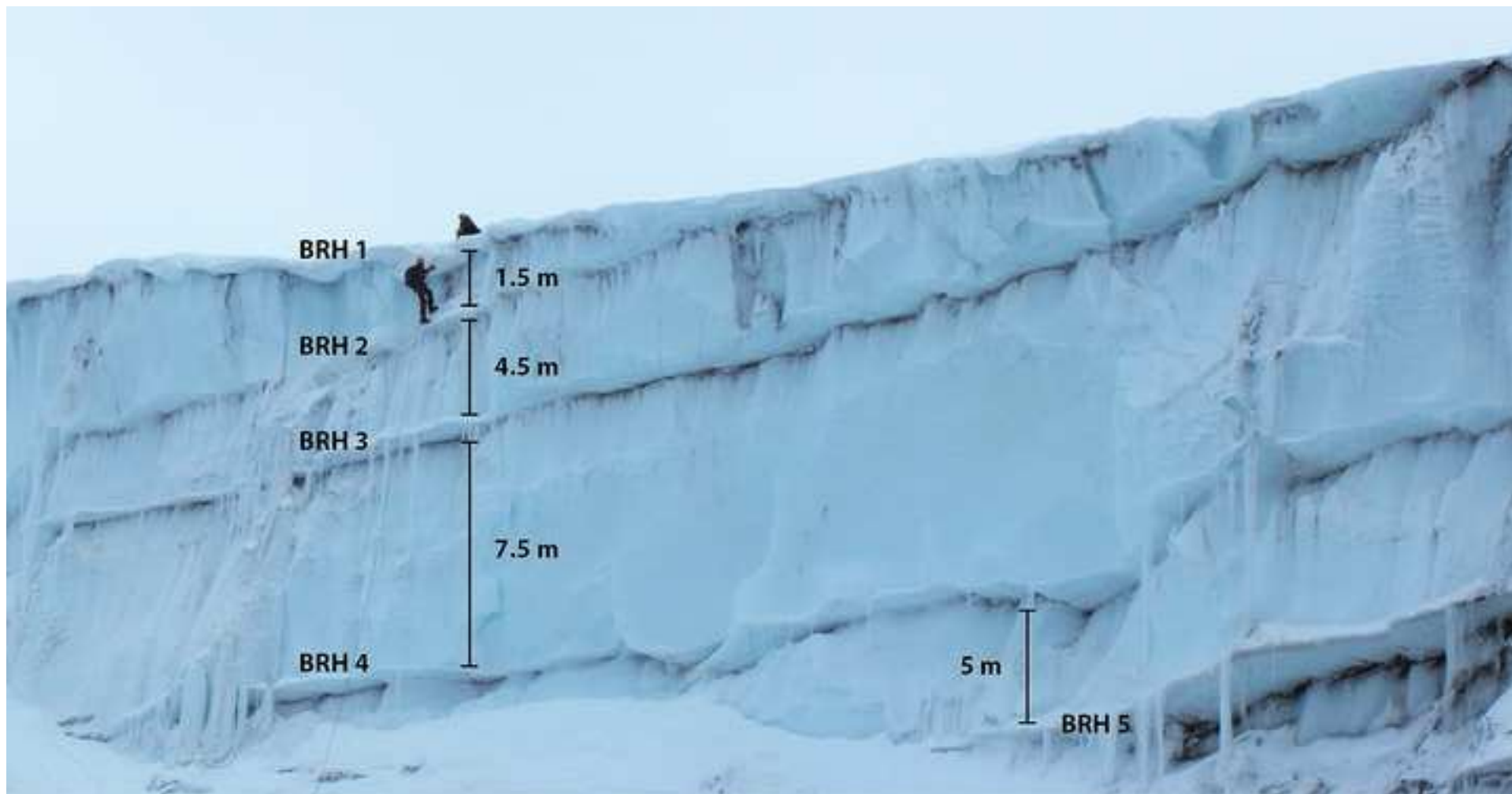
934 **Figure 7.** Bivariate trace element plots depicting the significant heterogeneity of the BRH1 to 5 tephra  
935 layers consistent with their major element variability ranging from basalts to trachytes. The plots  
936 illustrate the significant chemical overlap of these successive tephra deposits, which clearly lie upon  
937 an evolutionary trend indistinguishable from the products of Mount Melbourne (mainly trachytic),  
938 and offset from those of the nearby Mount Rittmann (after Del Carlo et al., 2022). The gray  
939 compositional field is for Edisto Inlet tephra TR17-08, whereas the black symbols indicate the  
940 average composition of Brimstone Peak tephra (+ BIT121, × BIT122; Dunbar 2003).  
941  
942

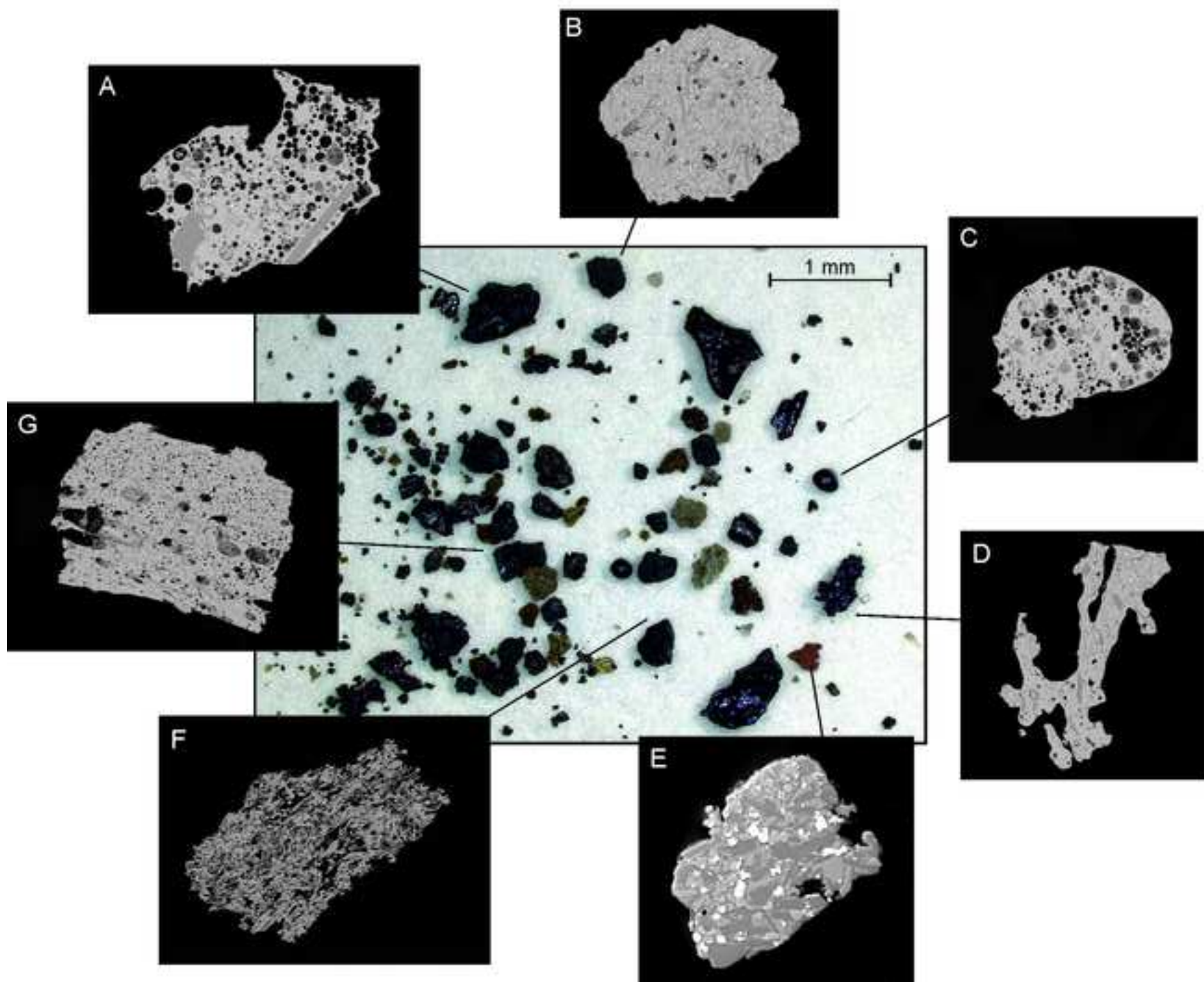
943 **Table 1:** Representative major, minor and trace element glass data for the BRH1 to 5 tephra deposits  
944 investigated. Bas = basalt; Bas Tra-And = basaltic trachy-andesite; Tra-And = trachy-andesite; Tra =  
945 trachyte. Full geochemical data sets are available in the Supplementary material file.

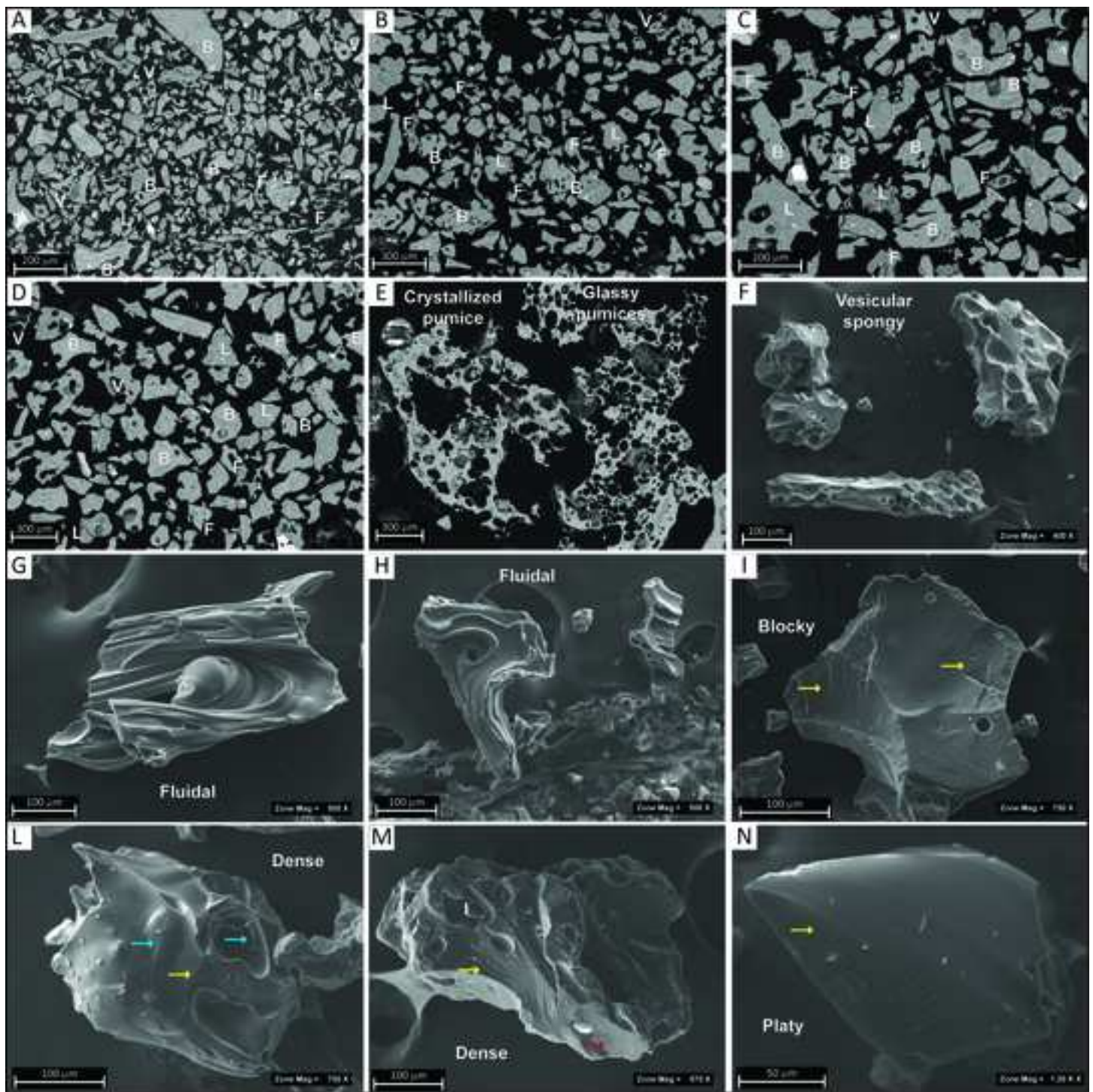
946

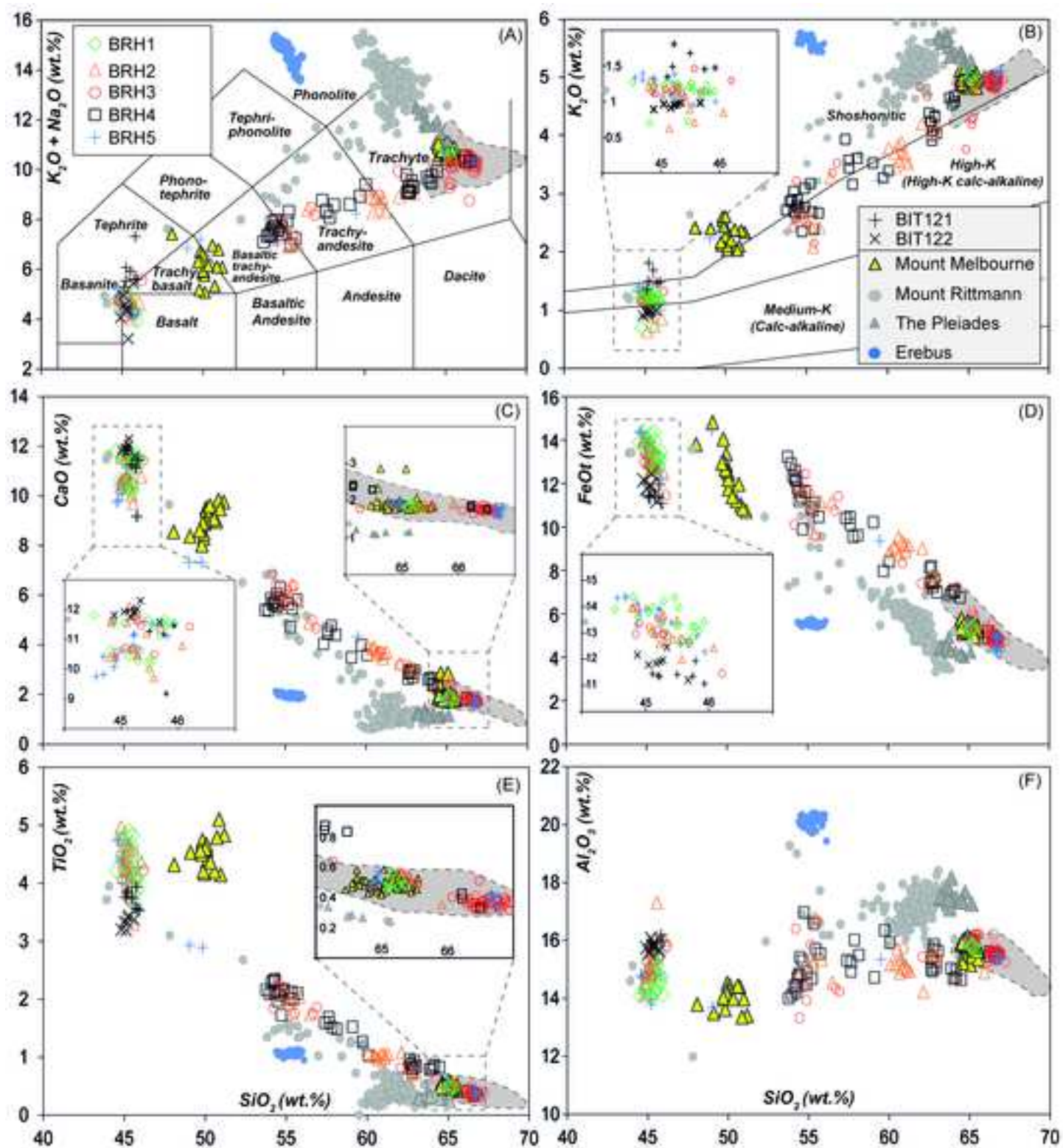
947 **Supplemental Information.** Geochemical data sets of major, minor and trace elements glass data for  
948 the BRH1 to 5 tephra deposits investigated.















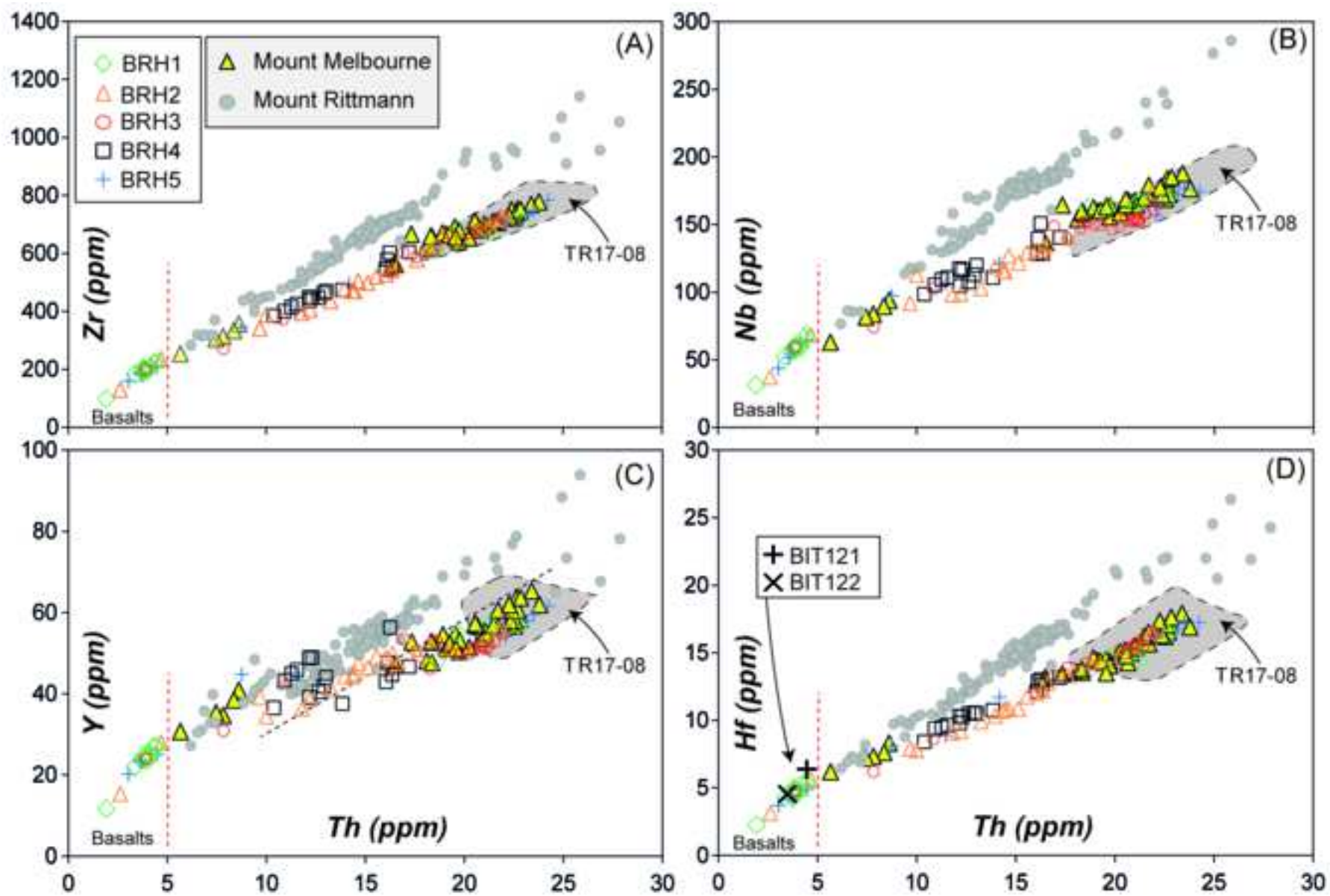


table 1

TAS Class. Norm. wt.%	BRH 1		BRH 2			BRH 3			BRH 4			BRH 5		
	Bas	Tra	Bas	Bas Tra-And	Tra-And	Basalt	Bas. Tra-And	Tra	Bas Tra-And	Tra-And	Tra	Bas	Tra	Tra
SiO <sub>2</sub>	45.52	65.11	45.27	55.28	61.09	45.28	54.70	66.67	54.45	57.63	64.13	45.17	64.85	66.77
TiO <sub>2</sub>	4.83	0.50	4.64	2.03	0.99	3.95	2.21	0.35	1.97	1.69	0.84	4.11	0.46	0.40
Al <sub>2</sub> O <sub>3</sub>	14.31	15.87	14.90	15.15	15.08	14.70	14.39	15.54	15.43	14.94	14.73	14.92	15.85	15.33
FeOt	13.96	5.30	13.61	11.46	8.88	12.98	11.66	4.76	11.21	10.44	6.99	12.87	5.68	4.85
MnO	0.15	0.11	0.21	0.25	0.19	0.17	0.25	0.12	0.19	0.21	0.21	0.15	0.16	0.17
MgO	5.12	0.16	5.24	2.04	0.81	6.12	2.07	0.16	1.91	1.50	0.60	5.94	0.21	0.19
CaO	10.21	1.85	10.45	5.97	3.65	11.61	5.95	1.78	6.05	4.60	2.37	11.70	1.92	1.80
Na <sub>2</sub> O	3.61	5.91	3.67	4.37	5.33	3.34	5.19	5.47	4.82	4.73	5.10	3.31	5.62	5.41
K <sub>2</sub> O	1.26	4.98	1.20	2.56	3.55	1.21	2.71	4.91	2.90	3.56	4.66	1.12	4.99	4.85
P <sub>2</sub> O <sub>5</sub>	0.94	0.03	0.74	0.78	0.31	0.56	0.77	0.04	0.96	0.55	0.20	0.64	0.04	0.07
Cl	0.08	0.19	0.06	0.11	0.12	0.07	0.10	0.19	0.13	0.14	0.17	0.06	0.22	0.18
Ana. Total	99.16	99.54	99.19	99.62	99.04	98.36	99.69	99.13	98.75	98.19	99.51	98.69	99.02	99.75
Na <sub>2</sub> O + K <sub>2</sub> O	4.87	10.89	4.87	6.93	8.88	4.56	7.90	10.39	7.71	8.29	9.76	4.43	10.62	10.26
<i>ppm</i>														
Rb	32.0	167.8	19.6	-	115.5	26.4	74.4	154.9	83.1	94.7	139.2	26.9	160.2	157.9
Sr	643	142	561	-	408	660	612	148	454	437	218	625	135	157
Y	27.0	54.4	15.3	-	47.5	23.8	42.9	51.8	48.8	44.1	46.7	23.0	56.8	54.0
Zr	222	687	128	-	504	197	373	685	449	469	605	189	709	711
Nb	68	165	37	-	127	59	102	152	118	120	141	54	165	157
Ba	371	1097	231	-	1052	328	831	1117	843	922	977	301	1044	1188
La	40.6	101.8	23.0	-	85.1	35.2	73.1	96.8	82.3	77.5	88.7	32.1	103.9	100.6
Ce	84.8	197.9	48.1	-	169.4	75.0	150.7	190.1	169.1	157.4	176.3	67.6	202.4	193.5
Pr	9.6	20.5	5.5	-	18.7	8.5	16.8	19.7	18.7	17.0	18.4	7.9	21.3	20.3
Nd	41.5	77.5	23.3	-	71.9	36.2	68.9	74.4	75.9	69.4	69.2	33.6	83.3	73.3
Sm	9.0	14.6	4.7	-	13.8	7.6	12.8	13.6	15.0	13.3	13.0	7.3	15.0	14.4
Eu	2.9	2.9	1.6	-	3.8	2.6	4.3	2.7	4.4	3.9	2.9	2.3	3.0	2.7
Gd	7.4	11.3	4.4	-	11.4	6.6	10.9	10.9	12.6	10.8	10.7	6.4	12.0	11.5
Dy	5.9	10.5	3.5	-	9.6	5.2	9.1	10.3	10.5	9.4	9.3	5.0	11.7	11.0
Er	2.7	5.7	1.6	-	4.7	2.5	4.3	5.4	5.0	4.5	4.7	2.5	6.1	5.8
Yb	2.3	5.4	1.2	-	4.3	1.8	3.6	5.5	4.2	4.3	4.7	2.0	5.6	5.4
Lu	0.3	0.7	0.2	-	0.6	0.3	0.5	0.7	0.6	0.6	0.6	0.3	0.8	0.8
Hf	5.3	15.1	3.1	-	10.8	4.7	8.6	15.4	10.3	10.5	13.2	4.5	16.2	16.1
Ta	4.1	9.2	2.2	-	6.7	3.6	5.9	8.6	6.6	6.8	7.7	3.2	9.1	8.9
Pb	2.3	23.8	1.4	-	14.8	1.9	8.7	18.7	9.2	11.3	16.1	3.0	19.3	19.2
Th	4.4	21.0	2.6	-	14.6	3.9	10.8	20.8	12.2	13.0	17.2	3.7	22.0	22.1
U	1.4	5.0	0.7	-	3.4	1.2	2.5	4.4	2.9	3.1	4.1	1.3	5.0	4.6
Zr/Th	50.4	32.6	49.1	-	34.4	50.9	34.4	32.9	36.9	36.1	35.1	51.5	32.2	32.2
Nb/Th	15.4	7.8	14.3	-	8.7	15.2	9.4	7.3	9.7	9.2	8.2	14.7	7.5	7.1
Y/Th	6.1	2.6	5.9	-	3.2	6.1	4.0	2.5	4.0	3.4	2.7	6.3	2.6	2.4



Click here to access/download  
**Supplementary Material**  
Supplemental Information-Revised.xlsx



*BUVO-D-23-00013 Title: Historical explosive activity of Mount Melbourne volcano (Antarctica) revealed by englacial tephra.*

Dear Editor,

please find below the reply to Editor's and reviewers' comments on the manuscript. We have accepted the suggestions that we believe have improved the paper, so we would like to thank them for their revision.

**Editor:** Of particular importance, you need to strengthen the arguments for the layers being primary tephras. This is fundamental. At present, you discuss this issue late on the paper (section 4.2). It needs to be moved to an earlier position and strengthened. The layers are highly unusual, being formed individually of several compositionally different sideromelane clasts. That might be explained by evacuation of a stratified chamber (you need to discuss this) but, as the reviewer suggests, it may also be due to surface reworking of several compositionally disparate sources. I have a field photo that shows the ice outcrop with your tephra layers and they seem to dip away from Baker Rocks as if they are successive ice bedload layers. Can you describe whether there is any abrasion of the clasts or are they so fragile & spinose that they cannot possibly be reworked (and are therefore primary)? You describe them as fall layers yet they sound like poorly sorted mixtures of ash & lapilli, which is not like fall (too much fine matrix). Can you clarify better why you think they are fall layers?

We agree. The “primary nature” of the layers only after the Results chapter since we would define (or confirm) their characteristics only after the textural and geochemical analysis. We have moved this section earlier to “3.1 Texture and components of tephra layers” just before the “Results” section, and refer back to it later in the paper.

In addition, in the Materials and methods chapter, we added a paragraph explaining that each sample is a “bulk” of the tephra layer thickness. In fact, due to the extreme sampling conditions, it was not possible to sub-sample each tephra layer at different stratigraphic heights and consequently study possible stratification with relative variation in grain size, composition, etc. relative to changes in the eruptive style, dynamics or in the composition of the magma feeding the eruptions. The samples were collected still embedded in the ice, which was then melted to recover the clastic fraction.

Again, as for the “primary nature” of the studied tephra, from the point of view of texture, we better highlight that glass fibres or Pele’s hairs were preserved in the deposits which is impossible in the case of re-sedimentation. The same for other fragile structures such as glass tips or glass coatings around crystals. In addition, particles show no rounding, abrasions, or surficial weathering, which is all indicative of re-sedimentation.

From the geochemical side, besides the glass composition of studied samples being bimodal or spread on a compositional field, these (especially on the trace elements variation diagrams) clearly plot on the same geochemical lineage indicating they are geochemically linked and derive all from the same volcanic system. We explained this in the Discussion chapter: “*The overall chemical variability (ranging from basalts through to trachytes) and in particular the observed clustering of the erupted volcanic glass compositions along the overall evolutionary trend might indicate that the successive eruptions were fed by a complex and vertically extensive magma storage region beneath the source volcano. Interestingly, apart from BRH4, all the remaining BRH tephra deposits comprise a basaltic glass component, and the interaction of the mafic melt with more evolved trachy-andesitic to trachytic magma pockets, or mush, is the likely trigger of these eruptions*”. This behaviour is quite frequent in many volcanic systems where explosive eruptions are fed by

bimodal magmas (e.g. basalts and trachytes), or by chemically zoned magma batch (covering a wide and continuous compositional spectrum). Just to mention some examples: Upper and Lower Pollara eruption, on Salina island, Aeolian Islands; several historical eruptions of La Palma, Canary Islands; most of the eruptions from Iceland volcanoes; Izu-Bonin Arc and many others.

Also, you use descriptors like 'Mt Melbourne volcanic complex' and 'Mt Melbourne volcanic province'. That is liable to cause confusion since the region has already been divided stratigraphically into the Melbourne Volcanic Province and the Mt Melbourne Volcanic Field (both part of the McMurdo Volcanic Group; see Sm & Rocchi, 2021 (GSL Mem)). If you disagree with that terminology, please discuss why, and how you are using your preferred terms.

We agree and have changed throughout.

I also recommend that you incorporate the results of the study by Smellie et al (2023; Frontiers - see annotated m/s). I know it wasn't published when you submitted your paper but that paper is relevant to your study and is now available.

Done.

Like the reviewer, I was also confused by the layout of the data in the supplementary table, so it needs better page/table descriptors (e.g. what are pages labelled 1, 2, 3, 4, 5?; what is 'MPI-DING?').

Done. Supplementary material has been reorganised, we added some references in it and explained the content. For instance, MPI-DING indicates the composition of standard glasses provided by Max-Planck-Institut für Chemie that are widely used as reference glasses in EPMA analyses.

**Reviewer #2:** The authors have a complicated and potentially interesting story here but much needs to be addressed and clarified for this paper to be ready to publish.

In the attached manuscript are a number of specific comments but I will summarize the main problems here.

More information is required for me to believe that each of these 5 layers are in fact tephra layers. These layers are undoubtedly made up of volcanic particles but more characterization is needed for them to become discrete and correlated tephra layers. Tephra is a general term for airborne pyroclastic material ejected during the course of a volcanic eruption (Thorarinsson, 1981). This could be a single eruptive event or multiple eruptions over a short period of time from the same vent.

See the comment above.

I am not sure these 5 layers are fall deposits from a single source. The bimodal compositions bother me. I do not see how the basalt and trachytes are linked to each other.

The composition of the particles in the layers are strangely similar despite not showing much chemical affinity or to each other. For instance in Layer 1, Ca is higher (~11 wt.%) in the basalt and considerably lower in the trachyte (~2 wt. %). There is only a small Eu anomaly.

See the comment above.

As can be clearly seen from the variation diagrams presented in the ms, the composition of each of the BRH tephra and those in the literature from Mount Melbourne define a clear and continuous evolutionary trend

from the basanite to trachyte composition fields. The basanite (which has a composition quite similar in all the studied samples) is the “parent” glass of the other compositions, in the sense that it represents the primitive term from which the more evolved compositions evolved (see comment above). This does not mean that trachyte X directly evolved from the basanite X contained in the same layers (see the comment just below, and have tried to explain this better in the discussion).

I think the authors need to show that there is geochemical evolution from one tephra layer to the other to confirm that each of the 5 trachytes evolved from a basalt to a trachyte over a very short period of time (100-200 years).

We have added in the ms: *“The overall chemical variability (ranging from basalts through to trachytes) and in particular the observed clustering of the erupted volcanic glass compositions along the overall evolutionary trend might indicate that the successive eruptions were fed by a COMPLEX AND VERTICALLY EXTENSIVE MAGMA STORAGE REGION BENEATH THE SOURCE VOLCANO...”* and that *“tephra deposits comprise a basaltic glass component, and the interaction of the mafic melt with more evolved trachy-andesitic to trachytic magma pockets, or mush, is the likely trigger of these eruptions.”*

Our interpretation is that a basanite magma TRIGGERED or REMOBLIZED multiple and different trachytic and trachy-andesitic magma batches that had already evolved and resided in different portions of the volcanic system of Mount Melbourne. This behaviour is typical in volcanic systems erupting both evolved and mafic terms (see for instance La Soufriere, La Martinica, Tenerife, etc.). Therefore, we do not understand these perplexities.

Would it be more reasonable to assume that there are multiple tephra from multiple volcanoes?

Literature data clearly show that the composition of Late Pleistocene to Holocene products of the other volcanoes of northern Victoria Land, such as The Pleiades or Mount Rittmann, plot on completely different chemical trend and clearly distinguishable from Mount Melbourne products (see Di Roberto et al. 2023 and references therein). The similar composition of the tephra presented in this paper is consistent with them being from the same source - Mt. Melbourne.

2) I am not sure the correlations and subsequent ages are robust enough. Cherry picking data to make it match distal tephra and then saying the basalt is missing because of distance and changes in winds is possible but not 5 times in a row. If there was basaltic data in the marine record then it would be more plausible. It would be great to correlate grain size with composition.

There is no “Cherry-picking” in the paper. We simply report that the tephra recently found in the Ross Sea sediments at Cape Hallett (Di Roberto et al. 2023) have IDENTICAL major and trace element compositions with two of the five tephra studied here (BRH3 and BRH5), but these lack the less evolved basanite component. Unless there is a very intense basaltic explosive eruption, it is quite difficult for basaltic ash to be dispersed more than a few tens of km from the source, and up to c. 280 km (the distance between Cape Hallett and Mount Melbourne). This is inherently linked to eruption dynamics, physical properties of basaltic magmas, plume height, etc. This is now discussed in more detail in the ms.

The differential distribution of ash with different compositions during a bimodal eruption is a common feature. An example is basaltic and rhyolitic ash dispersal in bimodal Icelandic eruptions.

Are all the basaltic particles larger than the fine ash?

In our deposits, the basaltic particles are always larger than trachytic pumices. We also specified in the ms that the mafic glass component is associated with the black glassy and fluidal particles.

3) I would like to see a more complete particle analysis comparing the size, shape and color of glass shards to composition. Is it completely mixed or are certain morphologies associated with specific compositions.

See comment above. The relation between texture and composition of different components is reported in the ms.

4) The supplemental material needs a lot more information. Here is a link to the Commission on Tephrochronology Community-based Recommendations for tephra data.

[https://www.google.com/url?q=https://earthchem.org/communities/tephra/&source=gmail-imap&ust=1682007225000000&usg=AOvVaw3OFzNt4J\\_J6qFP\\_2vpobuu](https://www.google.com/url?q=https://earthchem.org/communities/tephra/&source=gmail-imap&ust=1682007225000000&usg=AOvVaw3OFzNt4J_J6qFP_2vpobuu)

I would follow their templates on how to organize data and provide the necessary meta data.

I found it very difficult to connect the EPMA shard analysis to the LA-ICP-MS data and think more information is needed to connect these two data sets.

We have inserted a sentence within the LA-ICP-MS methods to clarify how the two datasets are connected. Where glass shards were individually mapped (gridded) within an epoxy mount, the analyses are labelled with a row letter (A, B, or C) and shard number. Doing so meant that we were able to ensure that EMP and LA-ICP-MS were conducted on precisely the same particle/shard. Consequently, the shard specific SiO<sub>2</sub> content (EMP analysis) was used as the internal standard for the LA-ICP-MS analysis and calculating the trace element contents.

Where individual glass shards were analysed within un-mapped (bulk) epoxy mounts, the average SiO<sub>2</sub> content of the relevant compositional components, was used as the internal standard to calculate the trace element contents. These average internal calibration values were assessed by monitoring the Si/Ca ratios from the EMP and LA-ICP-MS analyses.

In the supplementary information, we have highlighted the compositional classifications/component of the individual analyses in the EMP and LA-ICP-MS datasets, highlighting the sample averages, where used as the internal standard for the trace element analysis, making it clear how the dataset are integrated. We have also added a column in the trace element data sheet which clearly states the SiO<sub>2</sub> content converted to ppm and used as the internal standard, and again this can be traced to the major element datasheet.

5) The geochemical plots are way too busy. I would plot each layer separately and then make 1 plot with all of the data. The data presented for Mt. Melbourne is trachy-basalt and trachyte with nothing in between. The glass compositions in this paper run the whole composition range from basanite and basalt to trachyte. More data is needed to fill in the gaps. The only eruption I have seen with >20 wt% SiO<sub>2</sub> variation was Oruanui and it was only composed of ~1% basalt by volume.

We respectfully disagree. The overlapping chemical nature of the BRH deposits is an important feature well reflected in the existing plots, it demonstrates that the successive eruptions tap similar magma compositions and likely derive from the same volcanic source region. Successive plots for individual layers would require too many figures. We have inserted some zoomed-in captions to the plots to help better resolve some of the overlapping compositions, particularly in relation to data comparisons between the BRH and BIT tephtras.

In terms of the chemical heterogeneity, tapping of compositionally distinct, yet co-genetic, magmas is not uncommon, please see response above to the editors comments.



**Reviewer #3:** Dear Authors

I have read with interest your manuscript which provides compelling and strong data about recent tephras embedded within the Mt Melbourne ice glaciers and which may represent the deposits of the youngest preserved eruptions of this volcano, long debated as to be regarded as active and about the age of the last eruption. Geochemical correlations presented suggest that the tephra may be as young as the 3rd-4th century CE, which indeed would come as a clear indication of an active volcano. I have no comments about the dataset presented nor about the tentative age attribution which I find consistent also with the ice-stratigraphic evidence. I also agree with the authors that the summit area is not the likely source for these BRH tephra, as even if potentially buried beneath the ice filling the crater, the total lack of correlatable deposits on the summit crater rim makes it impossible for such young deposits to be originated in the summit region. I therefore agree that some lateral vent should be identified as the source and considering the young age I would expect to see the evidence of one or more hawaiian/strombolian edifice(s) to which the tephra may be correlated. Based on my personal experience may I suggest to consider the units ROL and SCC in Giordano et al 2012 as potential sources, both younger than 90ka but unfortunately not dated precisely. ROL is an extensive ropey basaltic lava field and SCC is a hawaiitic strombolian cone which both show no evidence of magma-ice interaction. The chemical characteristics and the eruption styles seem compatible, as well as the location, which is not far from the ice cliff where the BRH samples have been taken. I would recommend the authors to give a bit more space in the discussion to exploring where could the vent(s) be located along the Mt Melbourne flank and come up with some potential sources, as again the very young age of the tephra calls for their source identification

I hope these comments may be helpful

Guido Giordano

**We agree with Reviewer #3 and we added some sentences in the Discussion section suggesting the possible correlation between our tephra and the scoria cone around the Mount Melbourne volcano.**

We hope that we have fully addressed all the questions raised by the Reviewers. We also included in the ms the changes that were flagged on the annotated PDFs.

Best Regards

A. Di Roberto and co-authors